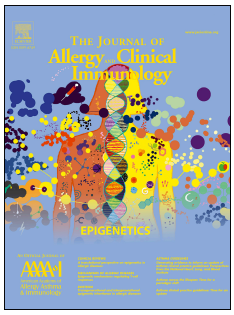
Journal Pre-proof



Belinostat resolves skin barrier defects in atopic dermatitis by targeting the dysregulated miR-335:SOX6 axis

Wen Chiy Liew, PhD, Gopinath M. Sundaram, PhD, Shan Quah, PhD, Lum Guo Guang, B.Sc., Jonathan S.L. Tan, B.Sc., Rajkumar Ramalingam, PhD, John E.A. Common, PhD, Mark B.Y. Tang, MD, E. Birgitte Lane, PhD, Steven Thng, MBBS, Prabha Sampath, PhD

PII: S0091-6749(20)30259-1

DOI: https://doi.org/10.1016/j.jaci.2020.02.007

Reference: YMAI 14424

To appear in: *Journal of Allergy and Clinical Immunology*

Received Date: 9 September 2019

Revised Date: 4 February 2020

Accepted Date: 7 February 2020

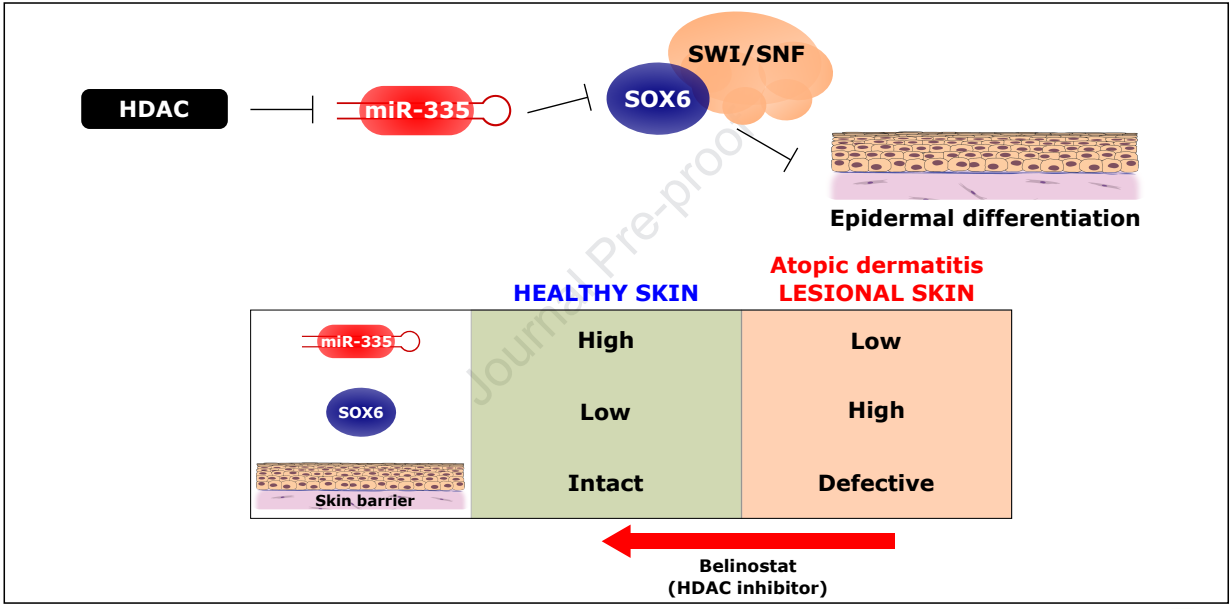
Please cite this article as: Liew WC, Sundaram GM, Quah S, Guang LG, Tan JSL, Ramalingam R, Common JEA, Tang MBY, Lane EB, Thng S, Sampath P, Belinostat resolves skin barrier defects in atopic dermatitis by targeting the dysregulated miR-335:SOX6 axis, *Journal of Allergy and Clinical Immunology* (2020), doi: https://doi.org/10.1016/j.jaci.2020.02.007.

This is a PDF file of an article that has undergone enhancements after acceptance, such as the addition of a cover page and metadata, and formatting for readability, but it is not yet the definitive version of record. This version will undergo additional copyediting, typesetting and review before it is published in its final form, but we are providing this version to give early visibility of the article. Please note that, during the production process, errors may be discovered which could affect the content, and all legal disclaimers that apply to the journal pertain.

© 2020 Published by Elsevier Inc. on behalf of the American Academy of Allergy, Asthma & Immunology.

Journal Pre-proof

Belinostat resolves skin barrier defects in atopic dermatitis by targeting the dysregulated miR-335:SOX6 axis



Journal Pre-proof

Abbreviations

HDAC: Histone deacetylase; SOX6: SRY-box transcription factor 6;
SWI/SNF: SWItch/Sucrose Non-Fermentable (a chromatin remodelling complex)

Journal Pre-proof

Belinostat resolves skin barrier defects in atopic dermatitis by targeting the dysregulated miR-335:SOX6 axis

Wen Chiy Liew, PhD[1,2,5], Gopinath M. Sundaram, PhD[1,2], Shan Quah, PhD[1], Lum Guo Guang, B.Sc.[1], Jonathan S.L. Tan, B.Sc.[1], Rajkumar Ramalingam, PhD[2], John E. A. Common, PhD[1], Mark B. Y. Tang, MD[3], E. Birgitte Lane, PhD[1], Steven Thng, MBBS[1,4], Prabha Sampath, PhD[1,5,6,*]

[1] Skin Research Institute of Singapore, Agency for Science Technology & Research (A*STAR), Singapore 138648

[2] Institute of Medical Biology, Singapore

[3] The Skin Specialists & Laser Clinic, Mt Alvernia Medical Centre, Singapore

[4] National Skin Center, Singapore

[5] Department of Biochemistry, Yong Loo Lin School of Medicine, National University of Singapore, Singapore

[6] Program in Cancer and Stem Cell Biology, Duke-NUS Medical School, 8 College Road, Singapore 169857

*Address for Correspondence

Prabha Sampath, PhD
Skin Research Institute of Singapore
Agency for Science Technology & Research (A*STAR)
8A Biomedical Grove, #05-41 Immunos,
Singapore 138648
+65-6407-0171

prabha.sampath@sris.a-star.edu.sg

Keywords: microRNA, atopic dermatitis, barrier defect, chronic inflammation.

Abbreviations: AD-atopic dermatitis, miR-335 -microRNA-335, 3'UTR- 3'-untranslated region, HDAC- histone deacetylases, LNA- locked nuclei acid, CE-cornified envelope, IVL-involucrin, SPRR- small proline rich proteins, TGM1-transglutaminase-1, ChIP -Chromatin immunoprecipitation and NaB -sodium butyrate.

Conflict of interest declaration: The authors have no conflicts of interest to disclose.

Journal Pre-proof

Abstract:

Background: Atopic dermatitis (AD) is a common chronic inflammatory skin disease. Skin barrier defects contribute to disease initiation and development, however underlying mechanisms remain elusive.

Objective: To understand the underlying cause of barrier defect, we investigated aberrant expression of specific microRNAs (miRNAs) in AD. Delineating the molecular mechanism of dysregulated miRNA-network, we focused on identification of specific drugs, which can modulate miRNA expression and repair defective barrier in AD.

Methods: A screen for differentially expressed miRNAs between healthy skin and AD lesional skin resulted in the identification of miR-335, as the most consistently downregulated miRNA in AD. Using *in silico* prediction combined with experimental validation, we characterized downstream miR-335 targets and elucidated the molecular pathways by which this microRNA maintains epidermal homeostasis in healthy skin.

Results: miR-335 was identified as a potent inducer of keratinocyte differentiation, and exerts this effect by directly repressing SOX6. Recruiting SMARCA complex components, SOX6 suppresses epidermal differentiation and epigenetically silence critical genes involved in keratinocyte differentiation. In AD lesional skin, miR-335 expression is aberrantly lost. SOX6 is abnormally expressed throughout the epidermis, where it impairs skin barrier development. We demonstrate that miR-335 is epigenetically regulated by histone deacetylases (HDACs), and a screen for suitable HDAC inhibitors identified belinostat as a candidate drug which can restore epidermal miR-335 expression and rescue the defective skin barrier in AD.

Conclusion: Belinostat is of clinical significance not only as a candidate drug for AD treatment, but also as a potential means of stopping the atopic march and further progression of this systemic allergic disease.

Journal Pre-proof

Capsule Summary:

Loss of epidermal microRNA, miR-335, causes skin barrier defects in atopic dermatitis. Belinostat, a histone deacetylase inhibitor, restores miR-335 expression and represents a potential therapeutic for treatment of atopic dermatitis.

Key messages:

- Loss of miR-335 causes barrier defects in atopic dermatitis.
- *SOX6,* a target of miR-355, suppresses epidermal differentiation via chromatin remodelling.
- Belinostat, a potential therapeutic for atopic dermatitis, restores miR-335 and rescue the defective barrier.

Journal Pre-proof

Journal Pre-proof

Introduction:

Atopic dermatitis (AD) is a chronic inflammatory skin condition (1, 2), which affects a significant proportion (15-30%) of children and 2-10% of adults. Symptoms include repeated episodes of skin inflammation, itching, scaling, and infection susceptibility, which severely diminish patients' quality of life. Key features of lesional skin from AD patients include skin barrier defects, compromised cornified envelope formation, and aberrant keratinocyte differentiation (3, 4).

Whilst skin lesions represent the most noticeable symptom of atopic dermatitis, much lies beneath the surface. AD is a complex systemic disease which is often the first indicator of 'atopic march' – the progression from atopic dermatitis to asthma and allergic rhinitis in affected individuals (5, 6). In this model, it is postulated that the epidermal barrier defect in AD causes excessive exposure to environmental aeroallergens, and that this allergen sensitization initiates the atopic march (7). The key role of epidermal barrier dysfunction in the origin of AD is a relatively recent finding; AD was initially thought to develop via immune dysregulation, with the skin barrier defect resulting from local inflammation (8). It is now known that a strong genetic association exists between AD and filaggrin (*FLG*) loss-of-function mutations (9). The filaggrin protein is expressed in the upper layers of the epidermis and exerts its function in cornified envelope formation and barrier function. AD lesional skin also shows reduced expression of other barrier function proteins such as filaggrin, loricrin and involucrin (IVL) (10). The evidence that a skin barrier defect predisposes patients towards AD presents an interesting opportunity for new therapeutic approaches to AD.

The development and maintenance of a healthy skin barrier is dependent on a number of factors, including translational control by microRNAs. MicroRNAs (miRNAs) are small, non-coding RNAs that mediate post-transcriptional gene regulation by targeting mRNAs for degradation and/or translational inhibition. Epidermal-specific deletions of key miRNA pathway components resulted in abnormal skin phenotypes, such as reduced barrier function and keratinocyte hyperproliferation in mice (11-13). Altered miRNA expression in

skin has been documented in systematic inflammatory diseases, including AD (14). However, the bulk of existing miRNA studies are either correlative (15, 16), or focus mainly on immune dysfunction (17-19). Here, we investigate microRNAs which are critical to maintain skin barrier function, and identify miR-335 as a key driver of keratinocyte differentiation and cornification. *In silico* predictions, followed by experimental validation, establish transcription factor SOX6 as a direct target of miR-335. This regulatory pathway, which promotes epidermal differentiation, is disrupted in AD. In healthy epidermis, miR-335 is abundantly expressed and SOX6 is absent. However, in AD skin lesions, loss of miR-335 is observed in tandem with aberrant SOX6 upregulation. SOX6 suppresses epidermal differentiation by recruiting SMARCA complex components, which epigenetically silence critical genes involved in keratinocyte differentiation. The resultant skin barrier defect can be therapeutically reversed by restoring miR-335 expression. We further demonstrate that miR-335 is epigenetically regulated by histone deacetylases (HDACs), and a screen for suitable HDAC inhibitors led to the identification of belinostat as a candidate drug which can restore epidermal miR-335 expression and ameliorate the associated barrier defect.

Journal Pre-proof

Methods:

Cell culture and transfection: N/TERT-1 keratinocytes were grown in keratinocyte serum-free medium (KSFM) (Life Technologies) supplemented with 0.2 ng/mL epidermal growth factor (EGF), 25 µg/mL bovine pituitary extract (BPE), 0.4 mM calcium chloride (CaCl2) and 1% penicillin/streptomycin. When high density cultures were required for experiments, N/TERT-1 cells were grown in DF-K medium of glutamine-free Dulbecco's modified Eagle's medium (DMEM; Gibco) and KSFM supplemented with 0.2 ng/ml EGF, 25 µg/ml BPE, 2 mM L-glutamine, 0.15 mM CaCl2 and 1% penicillin/streptomycin). HEK293T cells (Clontech) were cultured in DMEM supplemented with 10% fetal bovine serum (Gibco), 4 mM L-glutamine and 1 mM sodium pyruvate. Cultures were maintained at 37℃ in a humidified incubator containing 5% CO2.

N/TERT-1 keratinocytes were grown in six-well plates to 30-40% confluency before transfection. For miR-335 overexpression studies, N/TERT-1 cells were transfected with miR-335 mimic or negative control mimic (Dharmacon), at a final concentration of 30 nM using Lipofectamine® RNAiMAX reagent (Life Technologies) according to manufacturer's protocol. For knockdown studies, short interfering RNAs (siRNAs) against *SOX6*, *MEST*, *HELLS*, *SMARCA4*, *PNN* or *SMARCC1* (Dharmacon) were transfected into N/TERT-1 in the same manner as described for miRNA transfection. A non-targeting siRNA was transfected as negative control. Total RNA and/or protein were harvested at 48 hours post transfection and subjected to quantitative real time PCR and/or western blotting.

Patient recruitment and criteria used for biopsy collection: Standard 4 or 6 mm biopsies were obtained from 10 AD patients and 6 healthy individuals (male, aged between 20 and 40) in National Skin Centre, Singapore. Patients were recruited in a clinical study approved by National Healthcare Group Domain Specific Review Board (DSRB). Prior to biopsy collection, subjects were not given topical therapy for at least 2 weeks and systemic immunosuppressive treatment for at least 1 month. Biopsies were subjected to either RNA

Journal Pre-proof

extraction or neutral buffered formalin fixation for paraffin embedding. Control samples used were healthy skin sections from unrelated patients.

Preparation of lentiviral constructs, stocks and transduction: Lentiviral particles expressing shRNA targeting *SOX6* were prepared using an in house lentiviral vector, pLASH, which has features identical to pMIRZIP vector from System biosciences with minor modifications. Short hairpin RNA (shRNA) sequences were designed using InvivoGen siRNA Wizard^{TM} Software to target a 21-nt sequence within human *SOX6* (NM_033326). The oligos which form a stem loop upon annealing (sequences in Table. S2) were annealed (1F with 1R and 2F with 2R) and phosphorylated. pLASH vector was digested with restriction enzymes overnight, followed by gel purification. The gel purified-vector was then ligated with two annealed oligo pairs (Oligo pair 1 and 2) using T4 DNA ligase for 30 min and followed by transformation using One Shot TOP10 Chemically Competent *Escherichia coli* (ThermoFisher Scientific). Positive clones were selected based on a 1.8 kb fragment upon digestion with Xho1 restriction enzyme and further confirmed by Sanger sequencing.

Third-generation lentiviral particles were produced in HEK293T cells (Clontech) using calcium phosphate transfection, with co-transfection of lentiviral vectors and packaging mix made of three constructs, namely pMDLg/pRRE (#12251, Addgene), pRSV-Rev (#12253, Addgene) and pMD2.G (#12259, Addgene). Control viruses were prepared using empty vector constructs. For pTRIPZ plasmids, co-transfection was done with Trans-lentiviral packaging mix (Dharmacon) using Lipofectamine 2000 (Thermo Fisher Scientific) into HEK293T cells according to manufacturer's instructions. Viral particle-containing supernatants were harvested 48 hours and 72 hours after transfection. Viral supernatants were filtered through 0.22 µM membrane to remove non-adherent cells and debris, and subsequently concentrated via ultracentrifugation at 19600 rpm for 4 hours at 4℃. Viral particles were then re-suspended in Hank's Balanced Salt Solution (Sigma-Aldrich). To determine the titre of each virus, viral titration was performed in HEK293T cells after

transduction with serial dilutions of the lentiviral stocks according to the protocol described by Tiscornia *et al* (2006) (20). The viral titre was calculated based on the percentage of GFP-positive cells as revealed by flow cytometry analysis. Stably transduced cells were selected either using GFP sorting (for pCDH constructs) or using puromycin treatment (10 µg/ml) for 5 days (for pLASH constructs).

For over expression of SOX6, human SOX6 open reading frame (ORF) was amplified from pLenti-*SOX6* plasmid (RC212046, Origene) using primers listed in Table. S3. The forward primer used contains Myc tag (in italics) and hence the amplified fragment contains Myc tag at its 5' position in frame with *SOX6* ORF. The amplified fragment was then inserted into AgeI/MluI sites of pTRIPZ vector to generate pTRIPZ-*SOX6* (Primer sequences provided in Table. S3).

To generate the overexpression vector for hsa-miR-335, a 500 bp fragment spanning the precursor for hsa-miR-335 was amplified from human genomic DNA isolated from 293T cells. The miR-335 precursor was cloned downstream of the cytomegalovirus (CMV) promoter of pCDH-CMV-MCS-EF1-GFP lentiviral vector (System Bioscience) using XbaI and Eco RI restriction sites in the multiple cloning site (MSC).

miRNA profiling: Total RNA was extracted from skin biopsies using TRIzol® reagent followed by Exiqon miRCURY RNA column purification. Three technical replicates from control and lesional skin were subjected to microarray analysis. Total RNA was labelled using miRCURY LNA^{TM} microRNA Hi-Power Labelling Kit (Exiqon) according to manufacturer's protocol. The labelled samples were hybridized on the miRCURY LNA^{TM} microRNA Array (6th generation) with probes against 1223 known human mature miRNAs. Raw intensities from all samples were background subtracted, normalized using the global locally weighted scatterplot smoothing (lowess) regression method and $\log_2$ transformed. Differential miRNA expression analyses were performed using Partek Genomics Suite software.

Journal Pre-proof

Microarray analysis: Total RNA was converted to biotinylated cRNA using TargetAmp Nano-g Biotin-aRNA labeling kit (Epicenter). cRNA was purified using RNeasy Mini Kit (Qiagen). cRNA was hybridized on HumanHT-12 V4 Expression BeadChip Kit (Illumina) according to the manufacturer's instructions. The raw data was extracted, background subtracted and normalized using Illumina BeadStudio. Differential gene expression analysis was performed using Partek Genomics Suite software. Microarray data has been deposited in Gene Expression Omnibus database, accession no. GSE142135.

miRNA *in situ* hybridization: Paraffin-embedded skin tissue sections (5 µm) were dewaxed, rehydrated and boiled in pre-treatment solution (Panomics) for 5 minutes and subsequently treated with protease (Panomics) for 30 minutes at 37℃. Locked nucleic acid (LNA) probes purchased from Exiqon were added to the sections and incubated at 51℃ for 4 hours. The LNA probes used are specific to miR-335 and scrambled (non-targeting) sequences and are 5' and 3' digoxigenin- (DIG-) labelled. After washing the sections sequentially with 5X saline-sodium citrate (SSC), 1X SSC and 0.3X SSC buffer, they were blocked with 10% goat serum and incubated with anti-DIG alkaline phosphatase (Roche) overnight at 4℃. Fast Red Substrate (Panomics) was used to detect miRNA-bound LNA probes. Tissue sections were counterstained with 4',6-diamidino-2-phenylindole dihydrochloride (DAPI) (Sigma-Aldrich) and mounted with FluorSaveTM reagent (EMD Millipore). The slides were examined with an FV1000 inverted confocal microscope (Olympus) and images were acquired using Olympus FluoView with TRITC and DAPI filters.

Trans-epithelial electrical resistance: N/TERT-1 keratinocytes were seeded at a density of $0.5x10^6$/well in a 6-well tray 24 hours prior to transfection. Transfection was carried out using miR-335 mimics (Dharmacon™ Cat # C-300708-05) and control mimics (Dharmacon™ Cat # CN-001000-01-05) at a concentration of 30nM using Lipofectamine® RNAiMAX reagent (Life Technologies) according to manufacturer's protocol. The experiment was performed in triplicate. 24 hours post transfection, the cells were trypisnized and seeded

Journal Pre-proof

into 1.0µm 24-well inserts (corning, Cat No: 353103) in cDFK media. 24 hours post-seeding, medium was changed to cDFK enriched with calcium (to total of 1.6mM $CaCl_2$) and resistance readings were measured using TEER meter (EVOM2, World Precision Instrument). Resistance values are calculated and represented by Ω/cm^2 according to the user manual.

Immunohistochemistry: Paraffin wax-embedded skin tissue sections (5 µm) were dewaxed and rehydrated through an ethanol series. Endogenous peroxidase activity was quenched using 3% H_2O_2 in absolute methanol for 30 minutes. The sections were then boiled in antigen retrieval solution (pH 6, DAKO). Sections were then blocked in 10% goat serum for 30 minutes and incubated with primary antibodies overnight at 4℃. Secondary antibody incubation was carried out with anti-rabbit or -mouse Envision-labelled polymer reagents (DAKO) for 1 hour at room temperature. Staining was visualized using a 3,3'-diaminodbenzidine (DAB) substrate chromogen kit (DAKO). Slides were counterstained with haematoxylin and examined with a Zeiss AxioImager Z1 upright light microscope after mounting with CytosealTM60 mounting medium (Richard Allan Scientific). Images were acquired using Zeiss Zen software. Details of antibodies used in the study are provided in Table. S1

Immunocytochemistry: Cells were fixed and permeabilized with ice-cold acetone/methanol (1:1) for 10 minutes. After washing in phosphate buffered saline (PBS), the cells were incubated with 10% goat serum for 30 minutes. The cells were subsequently incubated with primary antibodies for 2 hours at room temperature or overnight at 4℃. After washing three times with PBS with 0.1% Tween 20, cells were incubated in dark with Alexa Fluor secondary antibodies (Invitrogen) for an hour. Nuclei were stained using DAPI. After washing with PBS, the cells were mounted onto slides with FluorSave reagent (EMD Millipore). Images were taken with an FV1000 inverted confocal microscope (Olympus) using Olympus FluoView. Details of antibodies used in the study are provided in Table. S1.

Quantitative real-time PCR: Total RNA was isolated using miRCURY™ RNA isolation kit (Exiqon). For miRNA quantification, cDNA was synthesized using Taqman® miRNA reverse transcription kit (Life Technologies) and the expression level of miRNAs was quantified by TaqMan Gene Expression Assays (Applied Biosystems) in 7900 fast RT-PCR system (Applied Biosystems) using Taqman miRNA-specific primers. For mRNA expression, cDNA was synthesized using SuperScript® III Reverse Transcriptase (Life Technologies) according to manufacturer's protocol. The expression levels of mRNAs were measured using SYBR green PCR Master Mix (Applied Biosystems). *U6* and *RPLP0* were used as endogenous normalization controls for miRNA and protein-coding genes, respectively. The expression of a gene/miRNA was defined from threshold cycle (Ct), and relative transcript abundance was calculated using ddCT method. All reactions were run in triplicate. The primers were designed using the Primer3 software and the NCBI design primer tools. The primers were checked for their GC content and any secondary structure formation using OligoCalc. Primer sequences are provided in Table. S5.

Western blotting: Whole cell lysates were extracted using RIPA buffer (50 mM Tris-HCl pH 7.4, 300 mM NaCl, 1% Nonidet P-40 (NP40), 1% sodium deoxycholate, 0.05% sodium dodecyl sulphate (SDS) and 10% glycerol) supplemented with protease inhibitor (Calbiochem). The concentration of the protein samples was measured by Bradford protein assay (Bio-Rad). 20-30µg protein samples were resuspended with 2x Laemmli buffer, separated on a 4-15% TGX™ precast protein gel (Biorad) by SDS-PAGE and electrophoretically transferred to PVDF membranes (Millipore). After incubation with 5% skimmed milk in Tris-buffered saline with 1% Tween (TBST) for 30 minutes, membranes were incubated with primary antibodies at 4℃ overnight. Membranes were washed three times for 15 minutes and incubated with HRP-conjugated anti-rabbit or anti-mouse antibodies. Blots were washed three times with TBST and developed through autoradiography using ECL western detection reagent (Millipore Crescendo). Beta-actin was

Journal Pre-proof

used as a protein loading control. Details of antibodies used in the study are provided in Table. S1.

Dual luciferase reporter assay: Luciferase reporter constructs containing the wild-type and mutant 3'UTRs of *SOX6* were purchased from GenScript. UTRs were subcloned from GenScript constructs into the Sac1/Xba1 sites of the pmirGlO dual-luciferase miRNA target expression vector. For the mutant 3'UTR, the miR-335 binding sequence (CTCTTG) was changed to CCTCCG. *SOX6* 3' UTR reporter constructs were co-transfected with pCDH or pCDH-335 plasmids into HEK293T cells using Lipofectamine 2000 (Thermo Scientific). The firefly and *Renilla* luminescence (normalization control) were detected 24 hours after transfection using Dual-Luciferase reporter assay (Promega).

Chromatin Immunoprecipitation: Cells were crosslinked with 1.5% formaldehyde for 10 minutes at 37℃. The reaction was stopped by adding glycine to a final concentration of 125 mM for 5 minutes at 37℃. Fixed cells were washed twice with ice-cold PBS, scraped and centrifuged. The pellets were then incubated with Buffer A (10 mM HEPES Ph7.9, 10 mM KCl, 0.1 mM EGTA, 1 mM DTT and 0.5 mM PMSF) supplemented with 1X protease inhibitor cocktail (Roche) and 10% glycerol on ice for 30 min, followed by 0.5% NP-40 for 5 minutes to lyse cytoplasmic membranes. The cells were then centrifuged at 1500 *g* for 5 minutes to pellet down nuclei. Nuclear pellet was then lysed in ChIP buffer (50 mM Tris pH 7.4, 150 mM NaCl, 5 mM EDTA, 0.5% NP-40, 1% Triton X-100, 0.05% SDS, 1× protease inhibitor cocktail). Nuclear chromatin was sheared by sonication for 15 min (30 sec on and 30 sec off) in a Bioruptor® water bath sonicator. The sonicated samples were centrifuged, and the supernatant containing the sheared chromatin was collected. For each ChIP reaction, 250 µl of chromatin extract was incubated with appropriate antibodies at 4℃ overnight on a rotary wheel. 50 µl of Protein A sepharose resin (precoated with 0.5% BSA and 0.2 mg/mL tRNA) was then added to the immunoprecipitated samples and incubated for 2 hours. The samples were then washed 5 times with ChIP buffer and the final wash was done with PBS. 100 µl of

Journal Pre-proof

10% Chelex slurry was added to each reaction and boiled for 5 minutes. The supernatant was collected, and the second elution was done with 100 µl nuclease-free water. The sample was then treated with RNase A (Roche) at 37°C for 2 hours followed by Proteinase K (Roche) at 55℃ overnight. The eluted samples were purified using the QIAquick PCR purification kit (Qiagen) according to the manufacturer's protocol. For total chromatin input, 25 µl of chromatin extract was washed with ice-cold 75% ethanol and spun at 16000 *g* for 10 minutes at 4℃. 100ul 10% Chelex slurry was added to each sample and boiled for 5 minutes. The eluted samples were then subjected to RNase A and Proteinase K treatment as described above. The resulting DNA was diluted 5X and 4 µl of each sample was used for real-time PCR. Fold enrichment of the genes was calculated using ddCt method with input Ct values as normalization control. Primer sequences are provided in Table. S4 and information on antibodies is in Table. S1.

Co-immunoprecipitation: Dynabeads Protein A (Invitrogen) were prepared according to the manufacturer's protocol. The nuclear lysates were incubated with DynaBeads Protein A coated with appropriate antibodies for 4 hours at 4℃. After washing the beads for 5 times in wash buffer (PBST) to remove non-specific proteins, the bead-bound proteins were analysed by mass spectrometry. For the validation of co-immunoprecipitated proteins by western blotting, proteins were eluted in 2x Laemli buffer at 95℃ for 5 minutes. The eluted proteins were analysed by immunoblotting using standard protocols. Information on antibodies included in Table. S1.

Mass spectrometry: Proteins bound to Dynabeads were digested following the protocol described in Sundaram *et al.* (21). The peptides were injected and separated using a Thermo ScientificTM Orbitrap FusionTM Mass Spectrometer (MS) and coupled nanoUPLC Easy LC 1000 with 120 min gradient (Solvent A: 0.1% formic acid, and solvent B: 0.1% formic acid with 99.9% of acetonitrile). Peak lists were generated with Proteome Discoverer (Version 1.4.1.14 Thermo Fisher Scientific), and protein identification was accomplished with

Mascot 2.5.1 against Human Uniprot database with following parameters: precursor mass tolerance (MS) 25 ppm, and MS/MS 0.6 Da, three missed cleavages; static modifications of Car- boamidomethyl (C), variable modifications are Biotin (K), Oxidation (M), Deamidation of (NQ). The candidates from three biological replicates presenting >2 unique peptides and >20 peptide-spectrum matches (PSM) were finally selected and subjected to experimental validation. The raw mass spectrometry datasets and curated SOX6 interacting partners have been submitted to the international standard data repository for proteomes (jPOSTrepo; Okuda et al., 2017) under accession no. https://repository.jpostdb.org/entry/JPST000713.

Cornified envelope assay: N/TERT-1 keratinocytes were grown in DF-K media until confluent, and then shifted to high Ca^{2+} conditions (1.5 mM) for a further 7 days in fresh DF-K media to induce terminal differentiation and cornified envelope formation, and the number of cornified envelopes (CEs) assessed following the method of Rice et al (22). In brief, cells were trypsinized and resuspended at 2.0 x 10^6 cells/ml in dissociation buffer containing 0.1 M Tris-HCl buffer pH 8.0, 2% SDS and 20 mM dithiothreitol. CEs were harvested by boiling the samples for 15 minutes at 100℃. Detergent- and reducing agent-resistant CEs were collected as an insoluble pellet by centrifugation at 4000×g for 10 minutes. CEs were counted with a hemocytometer, and CE formation was expressed as a percentage of input cell number.

Cap Analysis of Gene Expression (CAGE): CAGE tag analysis was performed using ENCODE data obtained from https://genome.ucsc.edu/ENCODE/. Tracks used for data analysis are: “RefSeq genes”, “NHEK whole cell PolyA+ CAGE +strand start sites” from ENCODE/RIKEN, “NHEK TAP-only whole cell small RNA-seq contigs” (+strand signal) from ENCODE/CSHL, “CpG islands”, “NHEK Pol2 Histone Mods by ChIP-seq peaks” from ENCODE/Broad, “NHEK EZH2 by ChIP-seq peaks” from ENCODE/Broad, “NHEK H3K27me3 by ChIP-seq peaks” from ENCODE/Broad, “NHEK H3K4me3 by ChIP-seq

peaks" from ENCODE/Broad, and "NHEK H3K9ac by ChIP-seq peaks" from ENCODE/Broad.

HDAC inhibitor screening: A panel of 42 HDAC inhibitors (HDACi) covering the majority of type I, II and pan HDACis were purchased from Selleckchem. N/TERT-1 grown to confluence were treated with HDACi at a final concentration of 1μM from a 100μM stock. Control wells were treated with DMSO at a final concentration of 1%. After 48hrs of treatment, cells were either processed for total RNA isolation or fixed and stained for human involucrin by immunocytochemistry.

***Ex vivo* human skin organ culture model:** Human skin organ culture was performed following Moll et al., (23). Briefly, clinically discarded abdominal skin from elective surgery was collected within 3hrs post-surgery, with informed consent of the patients. Excess fat was trimmed using scissors and 8mm circular explants were cut out using a commercial biopsy punch. Explants were placed on 6 well membrane inserts (4μM PET membrane) and cultured at air-liquid interface. HDAC inhibitors were dissolved in acetone at a final concentration of 1mM and 10μl of this mix was applied directly on the epidermal side of the biopsy and allowed to dry. Treatment with 10μl of acetone alone was used as mock treatment. Organ cultures were treated daily for a period of six days. After this period, skin biopsies were either processed for total RNA isolation as described earlier (24) or were fixed in 10% neutral buffered formalin and processed into FFPE sections.

Bioinformatics analysis software: DAVID (https://david.ncifcrf.gov/) was used to perform gene ontology. TargetScan (http://www.targetscan.org/), miRANDA (http://www.microrna.org) and PITA (https://genie.weizmann.ac.il/pubs/mir07/mir07_data.html) were used for miRNA target gene

prediction. ProteINSIDE (www.proteinside.org) was used to evaluate the enrichment of nuclear proteins in the mass spectrometry data set.

Statistical analysis: All quantitative data were presented as mean ± standard error. Statistical analysis was performed with two-tailed Student's *t* test when comparing two samples. Values of $p < 0.05$ were considered statistically significant.

Journal Pre-proof

Journal Pre-proof

Results:

A screen of miRNAs in AD identifies miR-335 as an epithelial differentiation factor: MicroRNA microarray analysis comparing AD lesional versus normal healthy skin revealed differentially-expressed miRNAs (Figure S1A, Table. S6). Microarray data were cross-checked using quantitative real-time PCR (qRT-PCR) on RNA isolated from 10 lesional skin samples and 6 healthy controls. miR-335 was the most consistent differentially-expressed miRNA in these samples, and is significantly downregulated in AD lesions relative to healthy skin (Student's t-test, $P < 0.01$; Figure. 1A). *In situ* hybridization on healthy and AD lesional skin revealed that miR-335 is abundantly expressed in healthy epidermis, but completely absent from AD skin lesions (Figure. 1B). In the healthy epidermis, miR-335 expression was significantly higher in the suprabasal (differentiating) layers relative to the basal (undifferentiated) layer (Figure 1B) suggesting a potential role of miR-335 in keratinocyte differentiation.

To investigate the role of miR-335, we transfected N/TERT-1 cells with miR-335 mimics. N/TERT-1 is an immortalized human keratinocyte cell line (25), which does not express miR-335 in its undifferentiated state (Figure. S1B, S1C). Cells transfected with control RNA or miR-335 mimics were assayed for their ability to show trans-epithelial electrical resistance (TEER assay). A significant increase in TEER was observed in N/TERT-1 cells transfected with miR-335 mimics, compared to control cells (Figure. S1D), suggesting that miR-335 enhances barrier integrity and tight junctions. This emphasizes the role of miR-335 in maintenance of the healthy epidermal barrier and implies that loss of miR-335 may contribute to barrier defects in AD.

To elucidate the underlying mechanism, total RNA from cells transfected with control or miR-335 mimics was subjected to microarray analysis and gene expression profile comparison. Gene set enrichment analysis revealed signatures of keratinocyte differentiation in N/TERT-1 cells transfected with miR-335 mimics. This included a subset of genes that were significantly enriched in GO terms related to keratinization and peptide cross-linking

Journal Pre-proof

(Figure. 1C). A cohort of genes essential for cornified envelope formation, including *IVL*, *SPRR1A*, *SPRR1B*, *SPRR2E*, *SPRR2F* and *TGM1,* genes in the epidermal differentiation complex on chromosome 1q, were significantly upregulated in N/TERT-1 cells expressing miR-335, compared to the control cells (Figure. 1D). Microarray results were further validated by qRT-PCR using biological replicates for this subset of genes with *RPLP0* as a normalization control. (Figure. 1E).

To confirm that miR-335 has a functional role in keratinocyte differentiation and cornification, we performed a cornified envelope assay on N/TERT-1 cells transfected with control or miR-335 mimics. Cornified envelopes are a well-established feature of terminal keratinocyte differentiation (26). They are formed by transglutaminase-catalyzed cross-linking of keratinocyte differentiation proteins, which includes involucrin (IVL), small proline rich proteins (SPRR) and other proteins. miR-335 significantly increased the number of cornified envelopes produced relative to the control (Figure. 1F and 1G), supporting our hypothesis that miR-335 is crucial for terminal keratinocyte differentiation.

***SOX6* is a direct target of miR-335:** To understand how miR-335 exerts its pro-differentiation role in epidermis, we analysed the downstream effectors of miR-335, using an integrated genomics, bioinformatics, and experimental approach. Hits from miRNA target prediction algorithms were cross-referenced with the list of transcripts downregulated in response to miR-335 from our microarray data. 30 transcripts fulfilling both criteria were shortlisted, including *SOX6* (Figure. 1D). *SOX6* transcript and protein abundance were both reduced in response to miR-335 transfection (Figure. 2A and 2B), as confirmed by qRT-PCR (normalized to *RPLP0*) and Western blot (β-actin as a loading control) analyses respectively. The 3' UTR of *SOX6* contains predicted binding sites for miR-335 (Figure. 2C). To confirm that S*OX6* is a direct target of miR-335, we cloned *SOX6* 3'-UTR into a luciferase reporter construct. Co-transfection of miR-335 mimics with *SOX6* wild-type 3'-UTR significantly reduced luciferase reporter activity (normalized to *Renilla* luciferase expression) and confirmed the binding of miR-335 to the target site in *SOX6* 3'-UTR. This interaction is

Journal Pre-proof

specific – we observed no change in reporter activity with a mutant 3'-UTR (Figure. 2D). In skin sections from healthy patients, a clear inverse correlation in the expression pattern of miR-335 and SOX6 was observed; intense nuclear staining for SOX6 in the basal layer of the epidermis coincides with little or no miR-335 (Figure 2E, upper panels). Suprabasal layers with significant miR-335 expression completely lacked SOX6. In AD lesional skin, where miR-335 expression is lost, nuclear SOX6 is expressed throughout the epidermis (Figure 2E, lower panels). In summary, all these data indicate that SOX6 is downstream target of miR-335.

miR-335 induces transcriptomic landscapes characteristic of epidermal differentiation by targeting *SOX6*: Having established *SOX6* as a direct target of miR-335, we set out to evaluate its functional role in the epidermis. Using specific short hairpin RNAs (shRNAs), we knocked down endogenous SOX6 in N/TERT-1 cells (Figure 3A and 3B). This substantially decreased cell proliferation (Figure. 3C and 3D). Genome-wide expression profiling of control and sh*SOX6* cells revealed differential expression of a subset of genes that were significantly enriched in GO terms related to terminal differentiation (epidermal development, differentiation, keratinization and peptide cross-linking) (Figure. 3E). Microarray results were validated by qRT-PCR using biological replicates for a subset of overlapping genes including *IVL*, *SPRR1A*, *SPRR1B*, *SPRR2E*, *SPRR2F* and *TGM1* (Figure 3F). These data show that SOX6 knockdown in N/TERT-1 cells phenocopies the effect of miR-335, validating that SOX6 is a downstream target suppressed by miR-335.

The transcriptomic response to SOX6 knockdown was reflected in the morphology of post-confluent sh*SOX6* keratinocytes. SOX6 knockdown increased cornified envelope production, providing further evidence that the absence of SOX6 facilitates differentiation (Figure. 3G). SOX6 downregulation is crucial for epidermal differentiation and healthy barrier formation.

To test our hypothesis that SOX6 inhibits epidermal differentiation by transcriptionally silencing genes essential for terminal differentiation, we screened promoters of genes with known roles in differentiation for consensus SOX6 binding sequences (27). We found putative SOX6 binding sites upstream of the transcription start sites in promoters of *IVL*, *SPRR2F* and *TGM1* genes. To study SOX6 occupancy at these sites, we subjected N/TERT-1 nuclear extracts to chromatin immunoprecipitation (ChIP) using antibodies against SOX6. Enrichment of SOX6 was found in the promoters of all three genes (Figure 3H). We confirmed the specificity of this interaction by showing that SOX6 is not enriched upstream of the control genes *RPLP0* and *KRT14*, which are expressed abundantly in epidermis (Figure. 3H). Moreover, inducible expression of SOX6 leads to substantial downregulation of involucrin as depicted by immunohistochemistry in an organotypic assay (Figure. S2). Together, these data support a model whereby SOX6 represses transcription in a subset of genes that are essential for epidermal differentiation (Figure. 3I).

SOX6 interacts with SMARCA chromatin remodelling complex and stalls epidermal cell differentiation: SOX6-mediated repression of keratinocyte differentiation may require additional interacting partners; SOX6 lacks a regulatory domain and interacts with other proteins to execute its functions (28). To identify SOX6-interacting partners, we generated HEK293T cell lines with doxycycline-inducible expression of SOX6 fused to an N-terminal MYC tag. Nuclear lysates from doxycycline-treated and untreated cells were immunoprecipitated with rabbit IgG, anti-SOX6 and anti-MYC antibodies (Figure. S3A).), and the precipitates analysed by mass spectrometry. After removing non-specific interactions, we obtained 26 putative SOX6-interacting proteins with known roles in transcriptional regulation and chromatin remodelling (Figure. S3B). These included several subunits of human *switch/sucrose non-fermentable* (SWI/SNF)-type ATP dependent chromatin remodelling complexes – SMARCA4 (BRG1), SMARCD2 (BRG1-associated factor; BAF60b), SMARCC1 (BRG1-associated factor; BAF155) and ACTL6a (BRG1-associated factor; BAF53a) (29) (Figure. 4A). HELLS (SMARCA6) was also identified as a

Journal Pre-proof

candidate SOX6 interacting partner. SWI/SNF complexes control the accessibility of DNA to transcription factors via nucleosome remodelling, thereby regulating (activation or repression of) target gene expression (30, 31). SWI/SNF proteins lack sequence specificity and interact with transcription factors to reach specific target sites. Therefore, we postulated that interaction of SOX6 with SMARCA proteins could facilitate recruitment of chromatin remodelling complexes (SWI/SNF) to specific genomic loci. Co-immunoprecipitation and co-localization confirmed the specific interaction of SOX6 with SMARCA4, SMARCA6 and SMARCC1 in keratinocytes (Figure. 4B). No co-localization was observed between SOX6 and the negative control protein Pinin 1 (PNN1). (Figure 4B). The extent of co-localization was quantified for all tested proteins by calculating the Pearson co-localization co-efficient in Z-stack confocal images (Figure. 4C). Immunoprecipitation with specific antibodies of SWI/SNF complex followed by western blot for SOX6 confirmed the interaction of SOX6 with SWI/SNF complex (Figure. S3C). Finally, loss-of-function studies support our model that interaction of SOX6 with SWI/SNF complex suppresses differentiation. Knockdown of *SMARCC1* significantly increases the expression of epidermal differentiation related genes *IVL*, *SPRR2F* and *TGM1* (normalized to *RPLP0*) (Figure. 4D).

In healthy skin, proliferating cells in the basal layer of the epidermis express very low levels of miR-335, leading to the expression of SOX6. By recruiting SMARCA complex components, SOX6 suppresses expression of epidermal differentiation factors in the basal layer of the epidermis. High levels of miR-335 observed in suprabasal layers will supress SOX6 expression, relieving transcriptional repression of *IVL*, *SPRR2F* and *TGM1*, and allowing keratinocyte terminal differentiation. However, epidermal miR-335 expression is lost in all layers of AD lesional skin. This absence of miR-335 allows sustained SOX6 expression throughout the epidermis (including suprabasal layers), leading to aberrant loss of proteins essential for differentiation. Epidermal differentiation is affected resulting in barrier defect and its associated contribution to allergen sensitization.

Epigenetic regulation of miR-335 by histone deacetylase 2 (HDAC2): According to our

Journal Pre-proof

model, defective barrier function in AD may be therapeutically addressed by restoring epidermal miR-335 expression. However, the molecular mechanisms governing miR-335 expression remain poorly understood. miR-335 is an intronic miRNA encoded within the second intron of mesoderm-specific transcript (*MEST*) (Figure. 5A). Intronic miRNAs can share the same promoters with their host genes or have their own separate promoters. Analysis of RNAseq data indicates that miR-335 is expressed in normal human epidermal keratinocytes cells. However, CAGE (Cap Analysis of Gene Expression) tags are only present in the upstream region of *MEST*, but not miR-335, suggesting that miR-335 does not have an independent promoter (Figure. S4).

Given the role of miR-335 in directing keratinocyte differentiation and its specific expression in suprabasal layers of epidermis, we investigated the expression of miR-335 in specific conditions which promote keratinocyte differentiation. Histone deacetylase (HDAC) inhibitors have been shown to induce keratinocyte differentiation and recent reports support their role in alleviating AD-like phenotypes in mouse models (32, 33). We observed that treating N/TERT-1 keratinocytes with sodium butyrate (NaB), a broad-spectrum HDAC inhibitor, caused significant miR-335 upregulation (Figure. 5B). NaB treatment also significantly increased *MEST* expression, supporting our hypothesis that miR-335 is transcribed in tandem with its host gene (Figure. 5C). A significant increase in the enrichment of H3K4ac at the upstream region of *MEST* and miR-335 upon treatment with NaB further supports a role of HDAC as a transcriptional regulator of both miR-335 and *MEST* (Figure. 5D).

Knockdown of *MEST* did not significantly affect expression of *KRT1* (a keratin expressed upon differentiation in suprabasal layers), *IVL*, or *TGM1* (Figure. 5E) confirming that only miR-335 mediates NaB-induced keratinocyte differentiation. On the other hand treatment with NaB leads to a significant upregulation of differentiation makers such as *IVL, SPRR2F* and *TGM1* (Figure. 5F). These observations suggest that NaB-induced HDAC inhibition enables expression of miR-335, which can exerts its pro-differentiation effects. By

inference, miR-335 suppression may result from HDAC activity, and the use of HDAC inhibitors to restore miR-335 expression in atopic dermatitis could represent a potential therapeutic strategy for restoring the skin barrier defect.

Belinostat restores barrier function and epidermal homeostasis via miR-335 network:

HDAC inhibitors (HDACi) can reprogram the cellular machinery to induce cell cycle arrest, differentiation and apoptosis, by altering the acetylation status of an array of substrates, including histones, transcription factors or chaperone proteins. Additionally, HDAC inhibitors can alter the expression profiles of miRNAs (34). Building on our results, that the HDAC inhibitor NaB can upregulate miR-335 and downstream genes essential for differentiation, we screened a panel of 42 HDAC inhibitors for their effects on stimulating keratinocyte differentiation, analysing their effects on IVL, SOX6 and miR-335 expression (Figure. S5). We first short-listed five HDAC inhibitors which can induce the expression of miR-335. One of these inhibitors, belinostat, significantly and consistently induces miR-335 expression in N/TERT-1 cells (Figure 6A). Belinostat-induced miR-335 expression was confirmed by *in situ* hybridization (Figure 6B, upper panel), and immunocytochemistry on N/TERT-1 cells showed significant IVL expression in the presence of this drug (Figure. 6B, lower panel). Belinostat also enhanced cornified envelope production compared to the control DMSO (Figure. 6C and 6D). These findings strongly suggest that belinostat is a potent inducer of miR-335 and could potentially restore the associated barrier defect in AD.

We tested the therapeutic potential of belinostat using an *ex vivo* human organ culture model, which simulates the AD phenotype. Punch biopsies from donor skin (with normal skin barrier function and a mature stratum corneum) were cultured at the air-liquid interface (23) and topically treated with either acetone (to provide a dry skin-like model), or HDAC inhibitors dissolved in acetone. We observed that belinostat induced significant expression of miR-335, when compared to other HDAC inhibitors (Figure. 6E). Belinostat-mediated miR-335 expression was confirmed using *in situ* hybridization (Figure. 6F). Immunohistochemical staining indicate IVL, which is downstream of miR-335 (Figure. 6G)

and filaggrin (FLG) (Figure. S6) were both upregulated upon treatment with belinostat. These findings provide evidence that belinostat can effectively induce epidermal miR-335 expression in a dry skin model, and potentially restore the barrier defect in atopic dermatitis.

Journal Pre-proof

Journal Pre-proof

Discussion:

Atopic dermatitis is a multifactorial disease with major contributions from the immune system and defects in skin barrier function that can exacerbate environmental percutaneous sensitization to drive atopy (35). A number of studies have previously reported microRNA (miRNA) dysregulation in AD; many such miRNAs are also known to be aberrantly expressed in other allergic disorders (36), whilst others are specific to AD (37). Here, we demonstrate the role miR-335, in the maintenance of epidermal homeostasis and loss of miR-335 in AD lesional skin. *In situ* hybridization reveals that miR-335 is abundantly expressed in the differentiated layers of healthy epidermis. This is consistent with previous reports that miR-335 showed higher expression in terminally differentiated keratinocytes compared to proliferating keratinocytes isolated from human skin (38). The role of miR-155 in AD immune dysfunction is well known , and notably, this group also detected miR-335 as being significantly downregulated in AD lesional skin (17). Our observation that miR-335 enhanced cornified envelope formation, by regulating the expression of specific differentiation-associated gene signature suggests that miR-335 is a critical regulator of keratinocyte differentiation. In AD lesional skin, downregulation of miR-335 abrogates expression of differentiation-related proteins such as IVL, SPRRs and TGM1, which disrupts differentiation and cornification, creating a barrier defect. Our study reinforces the hypothesis, that impaired barrier function initiates the atopic dermatitis through antigen penetration and allergen sensitization (9, 35).

However, the exact molecular mechanisms regulating AD pathophysiology remain elusive. We demonstrate that miR-335 exerts its pro-differentiation effect by suppressing *SOX6*. The transcription factor, *SOX6* is known to modulate terminal differentiation in mesoderm-, ectoderm-, and endoderm-derived cell lineages (39-41). Our data show that SOX6 is predominantly expressed in the proliferating basal layer of the healthy epidermis, where miR-335 expression is low. In AD lesional skin, where miR-335 expression is lost, the SOX6 expression domain expands into suprabasal layers. Aberrant expression of SOX6 transcriptionally represses genes related to keratinocyte differentiation and cornification.

In the absence of specific trans-activation or trans-repressor domain SOX6 interacts with various cofactors, such as components of the transcription machinery and chromatin remodelling proteins to execute its function. (42-45). Our results showed that transcriptional repression of specific genes associated with keratinocyte differentiation is mediated by the interaction of SOX6 with chromatin remodelling proteins SMARCA4, SMARCA6 and SMARCC1. Notably, SMARCA4 and SMARCC1 are part of a highly conserved multi-subunit chromatin remodelling complex known as the SWI/SNF family of proteins. The role of SWI/SNF complex in transcriptional repression of specific genes is well known (46, 47). Here we demonstrate spatio-temporal, SOX6-mediated transcriptional repression of specific differentiation associated genes by a distinct SWI/SNF complex.

Our data also suggests that miR-335 belongs to a cohort of miRNAs regulated by HDACs. (48, 49). We observed significant enrichment of HDAC1 and HDAC2 in the miR-335 promoter region, and noted that HDAC2 enrichment decreased upon treatment with the broad-spectrum HDAC inhibitor sodium butyrate. This also resulted in increased expression of differentiation-related markers including *IVL*, *TGM1* and *SPRR2F*. Consistent with these observations, other studies showed that treatments with HDAC inhibitors resulted in premature expression of differentiation markers (50, 51).

It is also possible that HDAC inhibitor effects are not limited to miR-335 regulation; SOX6 may also recruit HDACs to suppress target genes (52). Two independent studies have demonstrated that trichostatin A may suppress the development of AD-like symptoms in mice (32, 33). Recently it was demonstrated that, blocking HDAC activity using JNJ-26481585, a broad spectrum HDAC inhibitor is crucial to restore nasal mucosal function by promoting tight junction expression (53). This led us to hypothesize that HDAC inhibitors may be effective in treating AD, partly by upregulating miR-335 expression, which can induce differentiation-associated transcriptional signature and restore barrier function. Our screening assay resulted in the identification of belinostat, as a highly effective HDAC

inhibitor, that can potently restore both epidermal miR-335 and downstream keratinocyte differentiation-related genes.

Clinical trials are ongoing for three HDAC inhibitors intended for topical use in Mycosis fungoides cutaneous T-cell lymphoma (MF-CTCL) (54). The strategies adopted to ensure safety and minimal toxicity for these compounds provide insights on how this can be adapted for other HDAC inhibitors. We envision that development of a topical formulation for belinostat, which can ameliorate barrier defect and alleviate this chronic inflammatory skin condition.

Journal Pre-proof

Author Contributions: WCL and GMS performed most of the experiments, SQ performed drug screening assays, ISH and helped with TEER & bioinformatics, LGG performed TEER and IHC, JT contributed to IHC & ISH, RR helped in Mass spec, JC assisted with the explant experiment, MT supported us with the procurement of AD patient samples, EBL and ST helped us with data analysis. PS designed experimental plan, supervised the work and wrote the manuscript.

Acknowledgements: This work was supported by the Biomedical Research Council of Singapore and an Agency for Science, Technology, and Skin Innovation Grant (SIG18006).

Competing interests Declaration: The authors declare no competing interests.

Journal Pre-proof

References:

1. Weidinger S, Beck LA, Bieber T, Kabashima K, Irvine AD. Atopic dermatitis. Nat Rev Dis Primers. 2018;4(1):1.
2. Simpson ELMM, Irvine ADM, Eichenfield LFM, Friedlander SFM. Update on Epidemiology, Diagnosis, and Disease Course of Atopic Dermatitis. Semin Cutan Med Surg. 2016;35(5 Suppl):S84-8.
3. Agrawal R, Woodfolk JA. Skin barrier defects in atopic dermatitis. Curr Allergy Asthma Rep. 2014;14(5):433.
4. Trzeciak M, Sakowicz-Burkiewicz M, Wesserling M, Dobaczewska D, Glen J, Nowicki R, et al. Expression of Cornified Envelope Proteins in Skin and Its Relationship with Atopic Dermatitis Phenotype. Acta Derm Venereol. 2017;97(1):36-41.
5. Paller AS, Spergel JM, Mina-Osorio P, Irvine AD. The atopic march and atopic multimorbidity: Many trajectories, many pathways. J Allergy Clin Immunol. 2019;143(1):46-55.
6. Spergel JM, Paller AS. Atopic dermatitis and the atopic march. J Allergy Clin Immunol. 2003;112(6 Suppl):S118-27.
7. Hogan MB, Peele K, Wilson NW. Skin barrier function and its importance at the start of the atopic march. J Allergy (Cairo). 2012;2012:901940.
8. Boguniewicz M, Leung DY. Recent insights into atopic dermatitis and implications for management of infectious complications. J Allergy Clin Immunol. 2010;125(1):4-13; quiz 4-5.
9. Palmer CN, Irvine AD, Terron-Kwiatkowski A, Zhao Y, Liao H, Lee SP, et al. Common loss-of-function variants of the epidermal barrier protein filaggrin are a major predisposing factor for atopic dermatitis. Nat Genet. 2006;38(4):441-6.
10. Weidinger S, Novak N. Atopic dermatitis. Lancet. 2016;387(10023):1109-22.
11. Yi R, O'Carroll D, Pasolli HA, Zhang Z, Dietrich FS, Tarakhovsky A, et al. Morphogenesis in skin is governed by discrete sets of differentially expressed microRNAs. Nat Genet. 2006;38(3):356-62.
12. Andl T, Murchison EP, Liu F, Zhang Y, Yunta-Gonzalez M, Tobias JW, et al. The miRNA-processing enzyme dicer is essential for the morphogenesis and maintenance of hair follicles. Curr Biol. 2006;16(10):1041-9.
13. Yi R, Pasolli HA, Landthaler M, Hafner M, Ojo T, Sheridan R, et al. DGCR8-dependent microRNA biogenesis is essential for skin development. Proc Natl Acad Sci U S A. 2009;106(2):498-502.
14. Rozalski M, Rudnicka L, Samochocki Z. MiRNA in atopic dermatitis. Postepy Dermatol Alergol. 2016;33(3):157-62.
15. Specjalski K, Jassem E. MicroRNAs: Potential Biomarkers and Targets of Therapy in Allergic Diseases? Arch Immunol Ther Exp (Warsz). 2019;67(4):213-23.
16. Sonkoly E, Wei T, Janson PC, Saaf A, Lundeberg L, Tengvall-Linder M, et al. MicroRNAs: novel regulators involved in the pathogenesis of psoriasis? PLoS One. 2007;2(7):e610.
17. Sonkoly E, Janson P, Majuri ML, Savinko T, Fyhrquist N, Eidsmo L, et al. MiR-155 is overexpressed in patients with atopic dermatitis and modulates T-cell proliferative responses by targeting cytotoxic T lymphocyte-associated antigen 4. J Allergy Clin Immunol. 2010;126(3):581-9 e1-20.
18. Wang X, Chen Y, Yuan W, Yao L, Wang S, Jia Z, et al. MicroRNA-155-5p is a key regulator of allergic inflammation, modulating the epithelial barrier by targeting PKIalpha. Cell Death Dis. 2019;10(12):884.
19. Zeng YP, Nguyen GH, Jin HZ. MicroRNA-143 inhibits IL-13-induced dysregulation of the epidermal barrier-related proteins in skin keratinocytes via targeting to IL-13Ralpha1. Mol Cell Biochem. 2016;416(1-2):63-70.
20. Tiscornia G, Singer O, Verma IM. Production and purification of lentiviral vectors. Nat Protoc. 2006;1(1):241-5.

21. Sundaram GM, Ismail HM, Bashir M, Muhuri M, Vaz C, Nama S, et al. EGF hijacks miR-198/FSTL1 wound-healing switch and steers a two-pronged pathway toward metastasis. J Exp Med. 2017;214(10):2889-900.
22. Rice RH, Wong VJ, Pinkerton KE. Ultrastructural visualization of cross-linked protein features in epidermal appendages. J Cell Sci. 1994;107 (Pt 7):1985-92.
23. Moll I, Houdek P, Schmidt H, Moll R. Characterization of epidermal wound healing in a human skin organ culture model: acceleration by transplanted keratinocytes. J Invest Dermatol. 1998;111(2):251-8.
24. Sundaram GM, Common JE, Gopal FE, Srikanta S, Lakshman K, Lunny DP, et al. 'See-saw' expression of microRNA-198 and FSTL1 from a single transcript in wound healing. Nature. 2013;495(7439):103-6.
25. Dickson MA, Hahn WC, Ino Y, Ronfard V, Wu JY, Weinberg RA, et al. Human keratinocytes that express hTERT and also bypass a p16(INK4a)-enforced mechanism that limits life span become immortal yet retain normal growth and differentiation characteristics. Mol Cell Biol. 2000;20(4):1436-47.
26. Steven AC, Steinert PM. Protein composition of cornified cell envelopes of epidermal keratinocytes. J Cell Sci. 1994;107 (Pt 2):693-700.
27. An CI, Dong Y, Hagiwara N. Genome-wide mapping of Sox6 binding sites in skeletal muscle reveals both direct and indirect regulation of muscle terminal differentiation by Sox6. BMC Dev Biol. 2011;11:59.
28. Kamachi Y, Uchikawa M, Kondoh H. Pairing SOX off: with partners in the regulation of embryonic development. Trends Genet. 2000;16(4):182-7.
29. Sarnowska E, Gratkowska DM, Sacharowski SP, Cwiek P, Tohge T, Fernie AR, et al. The Role of SWI/SNF Chromatin Remodeling Complexes in Hormone Crosstalk. Trends Plant Sci. 2016;21(7):594-608.
30. Kadoch C, Crabtree GR. Mammalian SWI/SNF chromatin remodeling complexes and cancer: Mechanistic insights gained from human genomics. Sci Adv. 2015;1(5):e1500447.
31. Martens JA, Winston F. Recent advances in understanding chromatin remodeling by Swi/Snf complexes. Curr Opin Genet Dev. 2003;13(2):136-42.
32. Kim TH, Jung JA, Kim GD, Jang AH, Cho JJ, Park YS, et al. The histone deacetylase inhibitor, trichostatin A, inhibits the development of 2,4-dinitrofluorobenzene-induced dermatitis in NC/Nga mice. Int Immunopharmacol. 2010;10(10):1310-5.
33. Shi YL, Gu J, Park JJ, Xu YP, Yu FS, Zhou L, et al. Histone deacetylases inhibitor Trichostatin A ameliorates DNFB-induced allergic contact dermatitis and reduces epidermal Langerhans cells in mice. J Dermatol Sci. 2012;68(2):99-107.
34. Scott GK, Mattie MD, Berger CE, Benz SC, Benz CC. Rapid alteration of microRNA levels by histone deacetylase inhibition. Cancer Res. 2006;66(3):1277-81.
35. Cork MJ, Danby SG, Vasilopoulos Y, Hadgraft J, Lane ME, Moustafa M, et al. Epidermal barrier dysfunction in atopic dermatitis. J Invest Dermatol. 2009;129(8):1892-908.
36. Wu G, Yang G, Zhang R, Xu G, Zhang L, Wen W, et al. Altered microRNA Expression Profiles of Extracellular Vesicles in Nasal Mucus From Patients With Allergic Rhinitis. Allergy Asthma Immunol Res. 2015;7(5):449-57.
37. Chikh A, Matin RN, Senatore V, Hufbauer M, Lavery D, Raimondi C, et al. iASPP/p63 autoregulatory feedback loop is required for the homeostasis of stratified epithelia. EMBO J. 2011;30(20):4261-73.
38. Hildebrand J, Rutze M, Walz N, Gallinat S, Wenck H, Deppert W, et al. A comprehensive analysis of microRNA expression during human keratinocyte differentiation in vitro and in vivo. J Invest Dermatol. 2011;131(1):20-9.
39. Hagiwara N. Sox6, jack of all trades: a versatile regulatory protein in vertebrate development. Dev Dyn. 2011;240(6):1311-21.
40. Nachtigall PG, Dias MC, Carvalho RF, Martins C, Pinhal D. MicroRNA-499 expression distinctively correlates to target genes sox6 and rod1 profiles to resolve the skeletal muscle phenotype in Nile tilapia. PLoS One. 2015;10(3):e0119804.

41. Dugas JC, Cuellar TL, Scholze A, Ason B, Ibrahim A, Emery B, et al. Dicer1 and miR-219 Are required for normal oligodendrocyte differentiation and myelination. Neuron. 2010;65(5):597-611.
42. Lefebvre V, Li P, de Crombrugghe B. A new long form of Sox5 (L-Sox5), Sox6 and Sox9 are coexpressed in chondrogenesis and cooperatively activate the type II collagen gene. EMBO J. 1998;17(19):5718-33.
43. Han Y, Lefebvre V. L-Sox5 and Sox6 drive expression of the aggrecan gene in cartilage by securing binding of Sox9 to a far-upstream enhancer. Mol Cell Biol. 2008;28(16):4999-5013.
44. Liu CJ, Zhang Y, Xu K, Parsons D, Alfonso D, Di Cesare PE. Transcriptional activation of cartilage oligomeric matrix protein by Sox9, Sox5, and Sox6 transcription factors and CBP/p300 coactivators. Front Biosci. 2007;12:3899-910.
45. Murakami A, Ishida S, Thurlow J, Revest JM, Dickson C. SOX6 binds CtBP2 to repress transcription from the Fgf-3 promoter. Nucleic Acids Res. 2001;29(16):3347-55.
46. Choi J, Jeon S, Choi S, Park K, Seong RH. The SWI/SNF chromatin remodeling complex regulates germinal center formation by repressing Blimp-1 expression. Proc Natl Acad Sci U S A. 2015;112(7):E718-27.
47. Rao M, Casimiro MC, Lisanti MP, D'Amico M, Wang C, Shirley LA, et al. Inhibition of cyclin D1 gene transcription by Brg-1. Cell Cycle. 2008;7(5):647-55.
48. Koumangoye RB, Andl T, Taubenslag KJ, Zilberman ST, Taylor CJ, Loomans HA, et al. SOX4 interacts with EZH2 and HDAC3 to suppress microRNA-31 in invasive esophageal cancer cells. Mol Cancer. 2015;14:24.
49. Hsieh TH, Hsu CY, Tsai CF, Long CY, Wu CH, Wu DC, et al. HDAC inhibitors target HDAC5, upregulate microRNA-125a-5p, and induce apoptosis in breast cancer cells. Mol Ther. 2015;23(4):656-66.
50. Markova NG, Karaman-Jurukovska N, Pinkas-Sarafova A, Marekov LN, Simon M. Inhibition of histone deacetylation promotes abnormal epidermal differentiation and specifically suppresses the expression of the late differentiation marker profilaggrin. J Invest Dermatol. 2007;127(5):1126-39.
51. Leon Carrion S, Sutter CH, Sutter TR. Combined treatment with sodium butyrate and PD153035 enhances keratinocyte differentiation. Exp Dermatol. 2014;23(3):211-4.
52. Iguchi H, Urashima Y, Inagaki Y, Ikeda Y, Okamura M, Tanaka T, et al. SOX6 suppresses cyclin D1 promoter activity by interacting with beta-catenin and histone deacetylase 1, and its down-regulation induces pancreatic beta-cell proliferation. J Biol Chem. 2007;282(26):19052-61.
53. Steelant B, Wawrzyniak P, Martens K, Jonckheere AC, Pugin B, Schrijvers R, et al. Blocking histone deacetylase activity as a novel target for epithelial barrier defects in patients with allergic rhinitis. J Allergy Clin Immunol. 2019;144(5):1242-53 e7.
54. Lopez AT, Bates S, Geskin L. Current Status of HDAC Inhibitors in Cutaneous T-cell Lymphoma. Am J Clin Dermatol. 2018;19(6):805-19.

Journal Pre-proof

Figure Legends:

Figure. 1: A Screen of miRNAs in AD identifies miR-335 as an epithelial differentiation factor: A) Scatter plot representing relative miR-335 levels in healthy skin samples (n=6) versus lesional skin from AD patients (n=10). **B)** Expression of miR-335 detected by *in situ* hybridization in healthy versus AD lesional skin using specific probes against mature miR-335 or control probes. Inset in the middle panel shows magnified view of the epidermis, with basal layer demarcated by dotted lines. Scale bars = 100 µm. **C)** Gene ontology analysis on differentially regulated genes in N/TERT-1 cells expressing miR-335 in comparison with control cells. **D)** Heat-map of selected genes generated from microarray using RNA from N/TERT-1 cells transfected with miR-335 mimics or control RNA. Expression values displayed in shades of red (high) or blue (low) relative to the individual mean value of the gene in linear scale. **E)** Relative transcript abundance of *IVL*, *TGM1* and *SPRR*s in N/TERT-1 cells (n=3). **F)** Bar graph representing number of cornified envelopes in N/TERT-1 cells transfected with miR-335 mimics or control RNA and subjected cornified envelop assay (n=3). **G)** Representative phase contrast image of mature cornified envelopes. (**P<0.05 **P<0.01*; Student's t-test). Error bars denote ± s.e.m. NS = non-significant.

Figure. 2: *SOX6* is a direct target of miR-335: A) Relative transcript abundance of *SOX6* in N/TERT-1 cells transfected with miR-335 mimics or ~~a~~ scrambled control. **B)** Western blot showing relative levels of SOX6 in control cells or cells transfected with miR-335 mimics. β-actin was used as a loading control. **C)** The miR-335 binding site in the *SOX6* 3' UTR (sequence in blue). We mutated the seed sequence to disrupt the miR-335 binding site (in red). **D)** Bar graph showing normalized luciferase activity for N/TERT-1 cells co-transfected with wild-type or mutant luciferase reporter constructs, in the presence of miR-335 or control. Renilla luciferase was used as a normalization control. Luciferase activity is expressed as mean relative to controls (n= 3). ***p*< 0.001. Student's t-test was used to calculate *p* value and error bars denote ± s.e.m. **E)** *In situ* hybridization showing miR-335 expression (left

Journal Pre-proof

panels), on sections from healthy human skin (top) and AD lesional skin (bottom) (n=5). Immunohistochemical analysis of SOX6 (right panels), on sections from healthy skin (top) and AD lesional skin (bottom). In the upper panels, the basal layer is demarcated by dotted lines. Scale bars = 100 µm.

Figure. 3: Targeting *SOX6*, miR-335 induces transcriptomic landscapes characteristic of epidermal differentiation: A) Bar graph represents relative transcript abundance of *SOX6* in N/TERT-1 cells transduced with sh*SOX6* or Control RNA (n=3). **B)** Western blot showing relative levels of SOX6 in sh*SOX6* versus control, with β-actin as loading control. **C)** Representative phase-contrast images of N/TERT-1 cells transduced with sh*SOX6* or Control RNA. Scale bar = 100 µm. **D)** Cell-TiterGlo assay data for N/TERT-1 cells transduced with sh*SOX6* or control shRNA (n=3). **E)** Gene ontology analysis on differentially regulated genes upon *SOX6* knockdown in N/TERT-1 cells. **F)** Relative transcript abundance of genes essential for epidermal differentiation in response to sh*SOX6* or shControl (n=3). **G)** Number of cornified envelopes per field in N/TERT-1 keratinocytes transduced with shControl or sh*SOX6* (n=4) and values plotted as mean ± S.D. **H)** ChIP assay shows SOX6 occupancy on promoter regions of *IVL*, *TGM1* and *SPRR2F* represented as fold enrichment over control IgG, with *RPLP0* and *KRT14* as negative controls (n=3). **I)** Schematic depicting SOX6-mediated transcriptional suppression of *IVL*, *TGM1* and *SPRR2F* via a SOX6 binding motif in their promoters. (**P<0.05 **P<0.01*; Student's t-test). Error bars denote ± s.e.m. NS = non-significant.

Figure. 4: SOX6 interacts with SMARCA chromatin remodelling complex and stalls epidermal cell differentiation: A) List of selected, potential SOX6 interacting partners including subunits of SWI/SNF complex, detected by immunoprecipitation coupled mass spectrometry analysis. **B)** SOX6 co-localizes with SWI/SNF complex subunits. Immunocytochemistry on N/TERT-1 cells showing SOX6 (in green) co-stained with indicated subunit complexes (in red), namely, SMARCA6, SMARCA4 and SMARCC1. Z-stack images

were acquired and a representative image on a single plane is shown. Right panel depicts relative fluorescent intensities along the white line. Pinin 1 (PNN1), a nuclear protein, did not show significant colocalization with SOX6. **C)** To quantify the extent of colocalization, Pearson colocalization co-efficient was calculated using Z-stack images with Olympus FluoView software. Scatter plot shows the Pearson colocalization coefficient obtained for each gene pair (SOX6 vs SMARCA6/SMARCA4/SMARCC1/PNN1) from ~ 15 nuclei from 2 independent experiments. **D)** Relative transcript abundance of *IVL*, *SPRR2F* and *TGM1* mRNA levels in N/TERT-1 keratinocytes transiently transfected with a control siRNA or siRNA against *SMARCC1* (n=3). (**P<0.05 **P<0.01*; Student's t-test). Error bars denote ± s.e.m. NS = non-significant.

Figure 5: Epigenetic regulation of miR-335 by histone deacetylase 2 (HDAC2): A) Chromosomal location and genomic sequence of miR-335. miR-335 is located in the second intron of mesoderm-specific transcript (*MEST*) at the chromosome 7q32.2 locus. The stem loop sequence below indicates the precursor sequence of miR-335, with the mature sequence shown in green. **B)** Relative expression of miR-335 in N/TERT-1 cells treated with sodium butyrate (NaB). Ct values were normalized to U6 control. **C)** Relative expression of *MEST* in N/TERT-1 cells treated with NaB (n=3). *RPLP0* was used for normalization. **D)** Chromatin immunoprecipitation (ChIP)-qPCR for HDAC1, HDAC2 and H3K4ac occupancy at the shared promoter region of miR-335 and *MEST* in N/TERT-1 in the presence of NaB. Data are expressed as means ± SD (n=3). **E)** Relative transcript abundance of keratinocyte differentiation markers *KRT1*, *IVL* and *TGM1* in N/TERT-1 cells upon *MEST* knockdown (n=3). **F)** Relative transcript abundance of *IVL, SPRR2F* and *TGM1* in N/TERT-1 cells treated with NaB. *RPLP0* was used for normalization. Data are representative of three independent experiments and plotted as mean ± S.D. (**P<0.05 **P<0.01*; Student's t-test). Error bars denote ± s.e.m. NS = non-significant.

Journal Pre-proof

Figure. 6: Belinostat restores barrier function and epidermal homeostasis via miR-335 network: A) Bar graph represents miR-335 expression in N/TERT-1 cells upon treatment with HDAC inhibitors (n=3). **B)** N/TERT-1 cells were treated with belinostat or DMSO (control). *In situ* hybridisation showing miR-335 expression (red, top panels). Immunocytochemistry showing involucrin expression (red, bottom panels) (n=3). **C)** Bar graph representing number of cornified envelopes per field in N/TERT-1 cells treated with belinostat or DMSO (n=4). **D)** Representative phase contrast images of cornified envelopes from N/TERT-1 cells treated with belinostat or DMSO. **E)** miR-335 expression in human skin biopsies topically treated with acetone alone, or HDAC inhibitors dissolved in acetone (n=3). **F)** *In situ* hybridisation showing miR-335 expression in human skin biopsies that were topically treated with acetone alone or belinostat dissolved in acetone (n=3). **G)** Immunohistochemical analysis of IVL, on sections from human skin biopsies that were topically treated with acetone alone or acetone + belinostat (n=3). Student's t-test was used to calculate *p* value * p-value < 0.05, ** p-value < 0.001. Scale bars, 50 µm. **H)** Model depicting how miR-335 loss can lead to dysregulated molecular pathways promoting AD. Schematic representation of restoration of epidermal homeostasis upon treatment with belinostat.

Journal Pre-proof

Figure.1

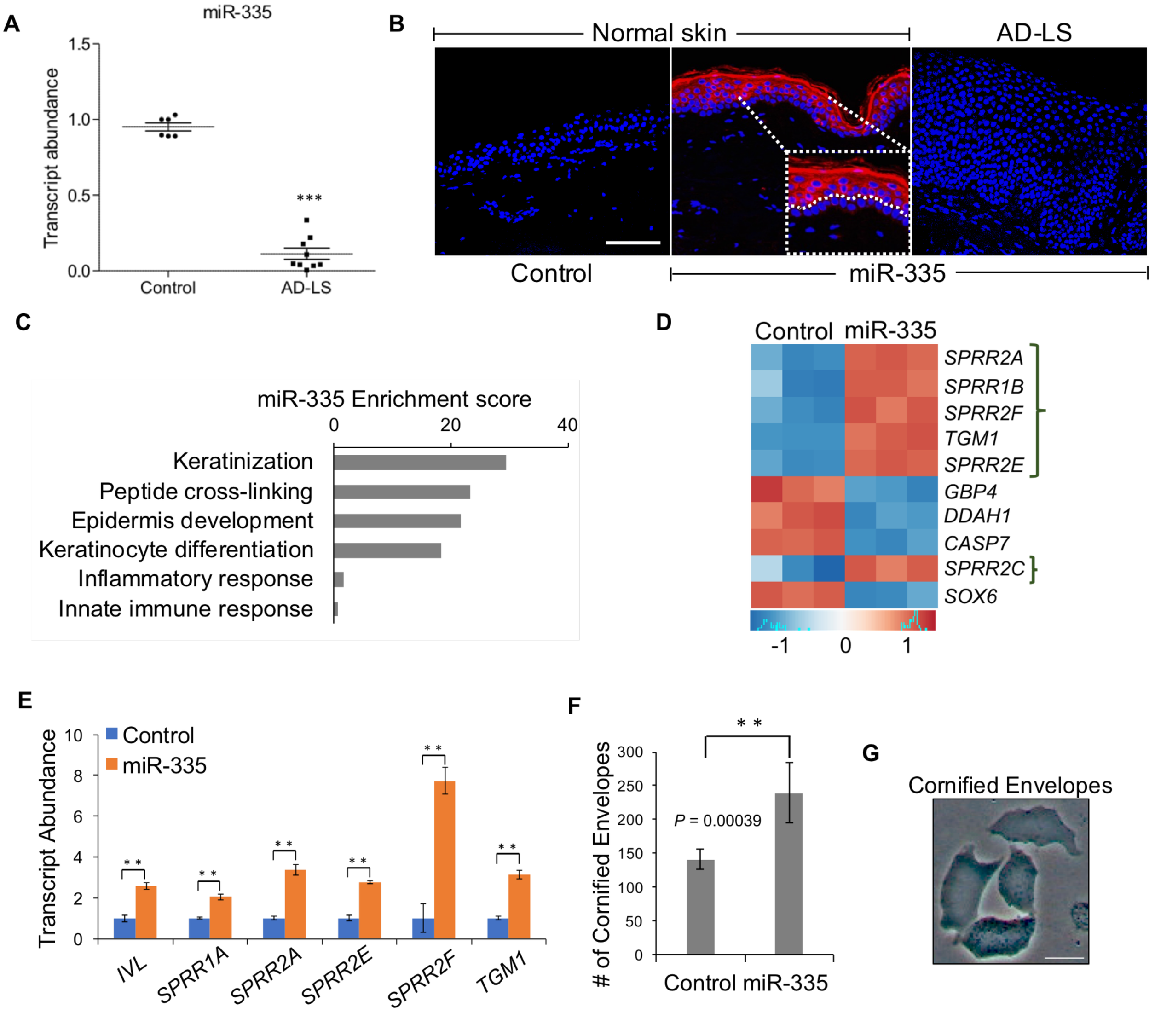
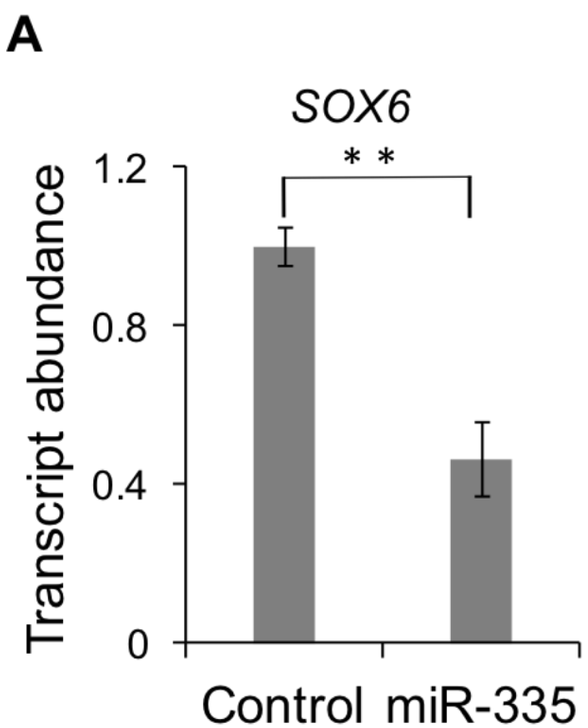
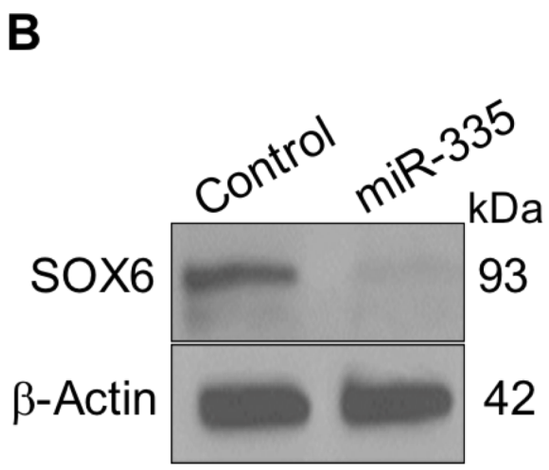
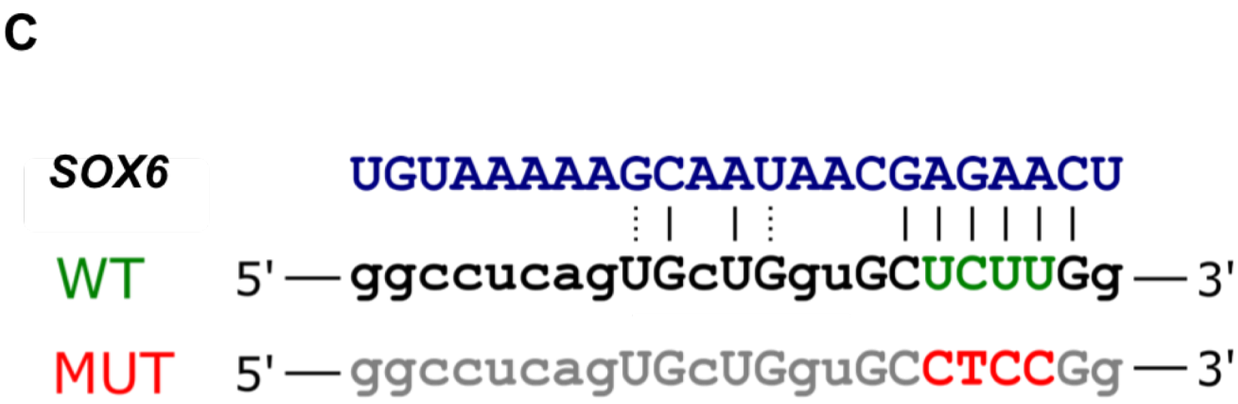
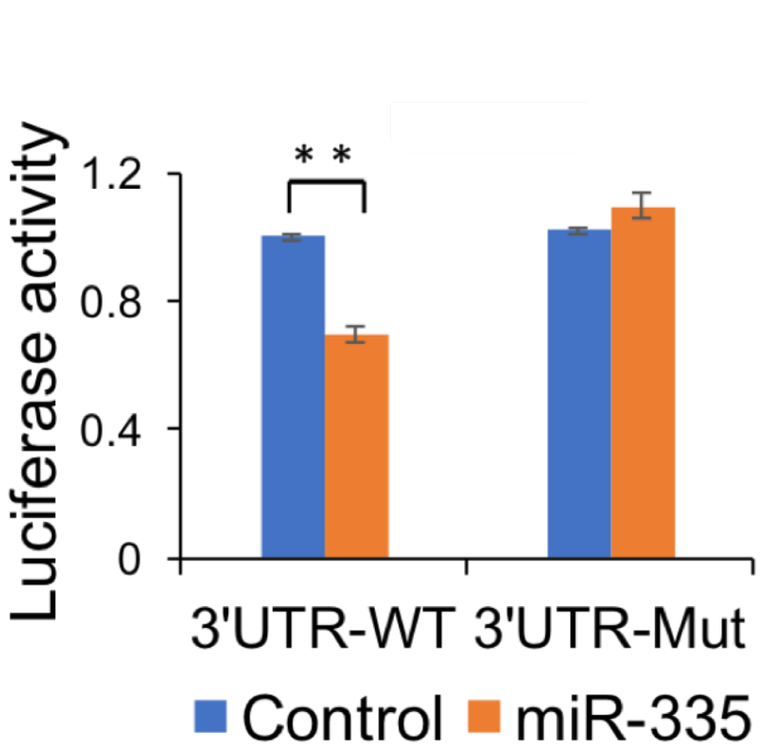

A
miR-335
Transcript abundance
1.5
1.0
0.5
0.0
***
Control
AD-LS
B
Normal skin
AD-LS
Control
miR-335
C
miR-335 Enrichment score
0
20
40
Keratinization
Peptide cross-linking
Epidermis development
Keratinocyte differentiation
Inflammatory response
Innate immune response
D
Control
miR-335
SPRR2A
SPRR1B
SPRR2F
TGM1
SPRR2E
GBP4
DDAH1
CASP7
SPRR2C
SOX6
-1
0
1
E
Transcript Abundance
Control
miR-335
10
8
6
4
2
0
* *
IVL
SPRR1A
SPRR2A
SPRR2E
SPRR2F
TGM1
F
of Cornified Envelopes
300
250
200
150
100
50
0
* *
P = 0.00039
Control
miR-335
G
Cornified Envelopes

Figure. 2


A
SOX6
* *
Transcript abundance
1.2
0.8
0.4
0
Control
miR-335


B
Control
miR-335
kDa
SOX6
93
β-Actin
42


C
SOX6
UGUAAAAAGCAAUAACGAGAACU
WT
5' — ggccucagUGcUGguGCUCUUGg — 3'
MUT
5' — ggccucagUGcUGguGCCTCCGg — 3'


D
Luciferase activity
* *
1.2
0.8
0.4
0
3'UTR-WT
3'UTR-Mut
Control
miR-335

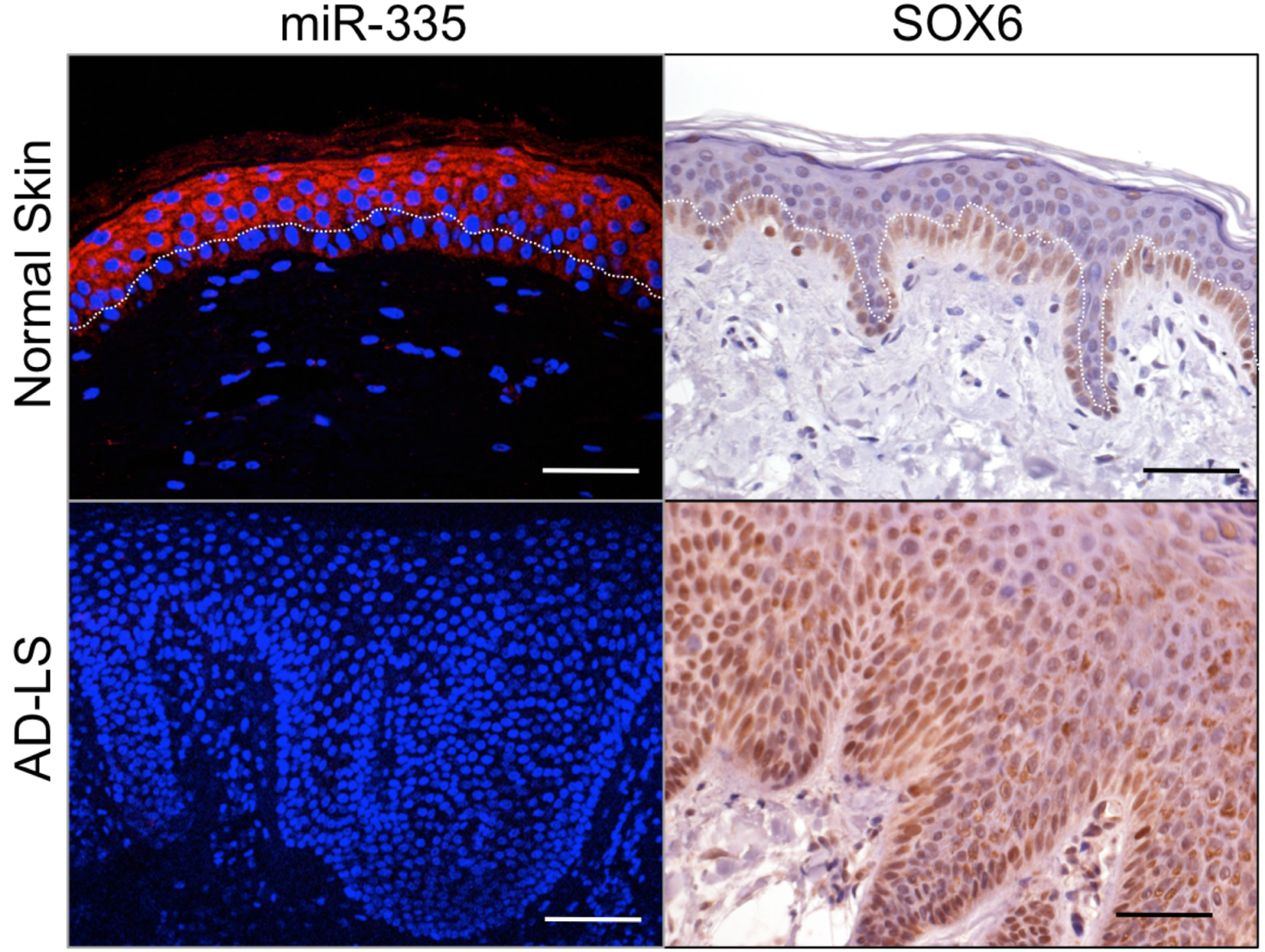
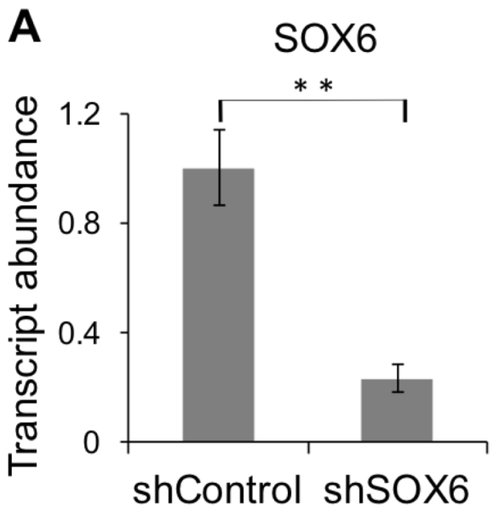
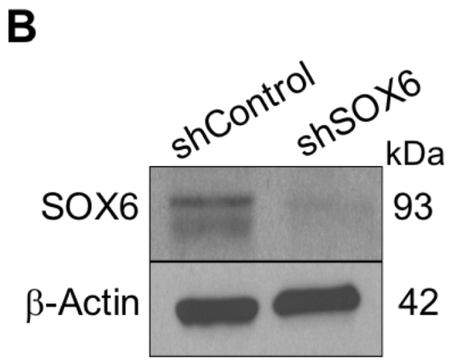
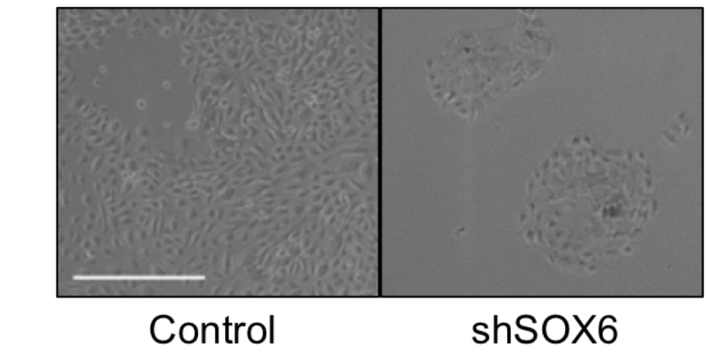
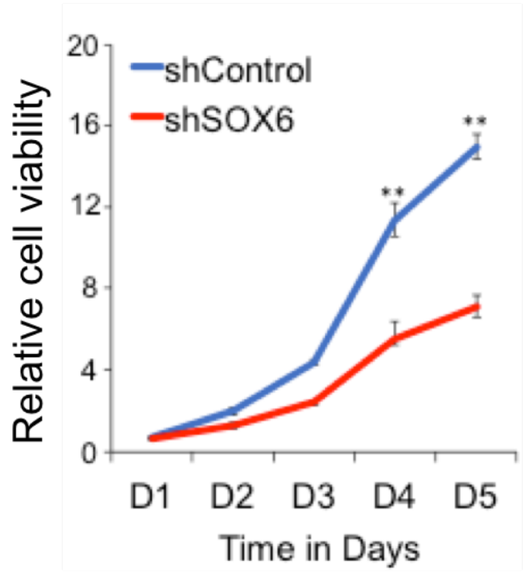

E
miR-335
SOX6
Normal Skin
AD-LS

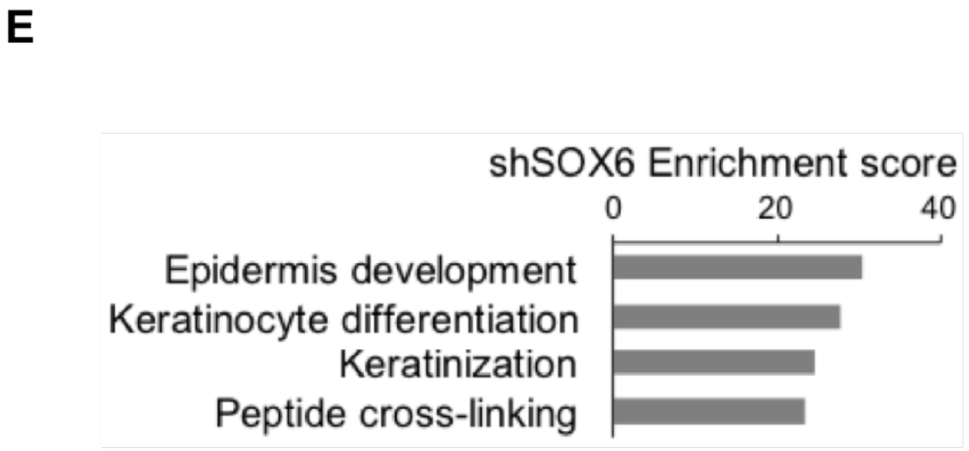
Figure. 3

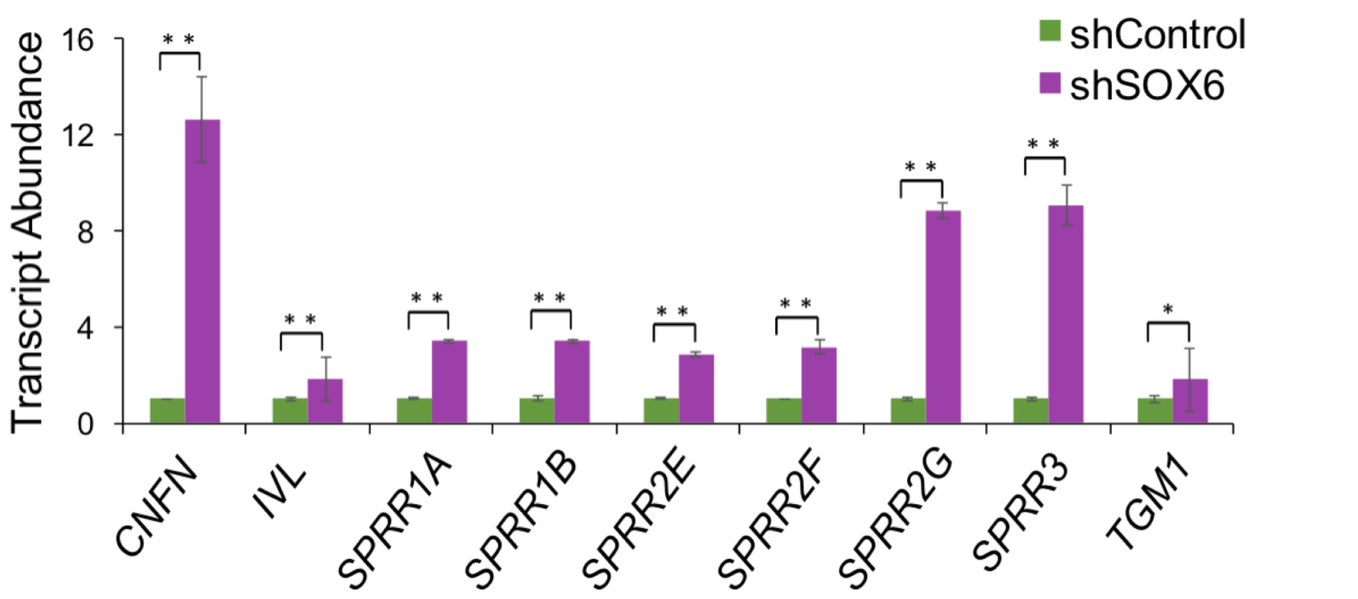

A
SOX6
* *
Transcript abundance
1.2
0.8
0.4
0
shControl
shSOX6

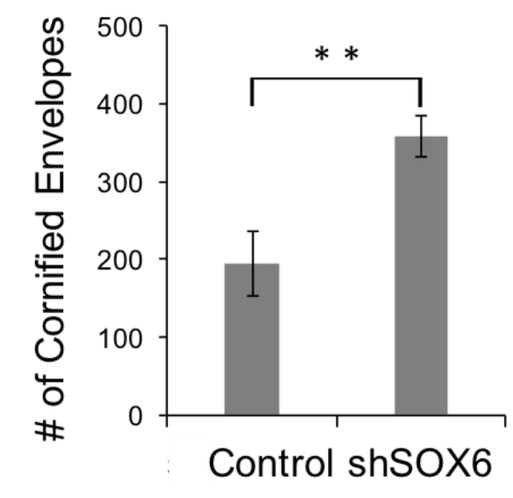

B
shControl
shSOX6
kDa
SOX6
93
β-Actin
42

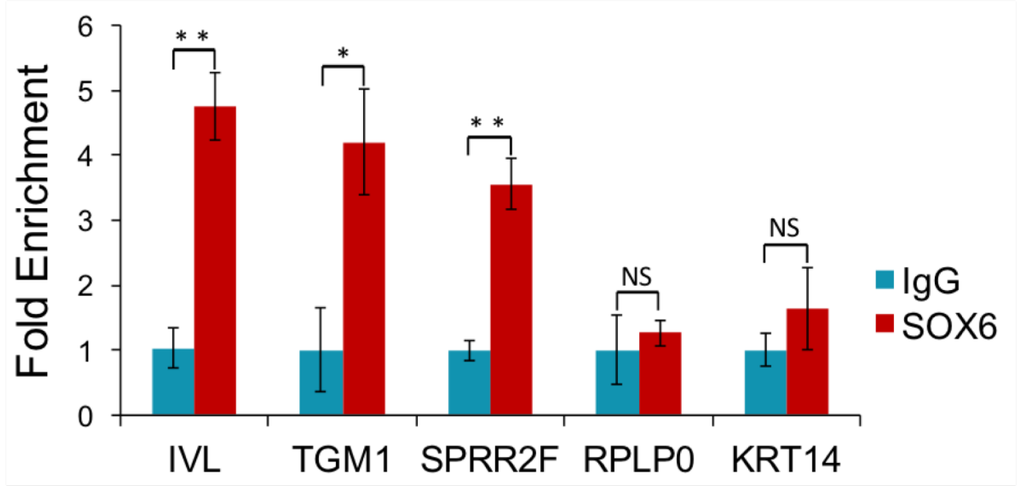

C
Control
shSOX6


D
shControl
shSOX6
Relative cell viability
20
16
12
8
4
0
**
**
D1
D2
D3
D4
D5
Time in Days


E
shSOX6 Enrichment score
0
20
40
Epidermis development
Keratinocyte differentiation
Keratinization
Peptide cross-linking


F
shControl
shSOX6
Transcript Abundance
16
12
8
4
0
* *
*
CNFN
IVL
SPRR1A
SPRR1B
SPRR2E
SPRR2F
SPRR2G
SPRR3
TGM1


G
of Cornified Envelopes
500
400
300
200
100
0
* *
Control
shSOX6


H
Fold Enrichment
6
5
4
3
2
1
0
* *
*
* *
NS
NS
IgG
SOX6
IVL
TGM1
SPRR2F
RPLP0
KRT14

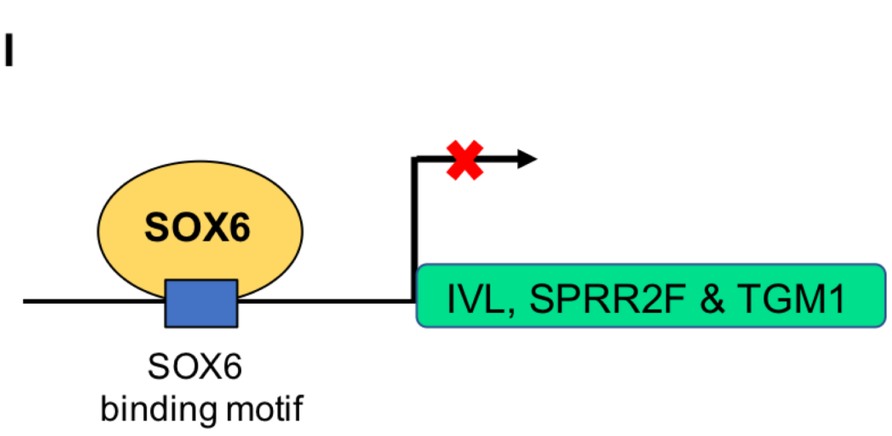
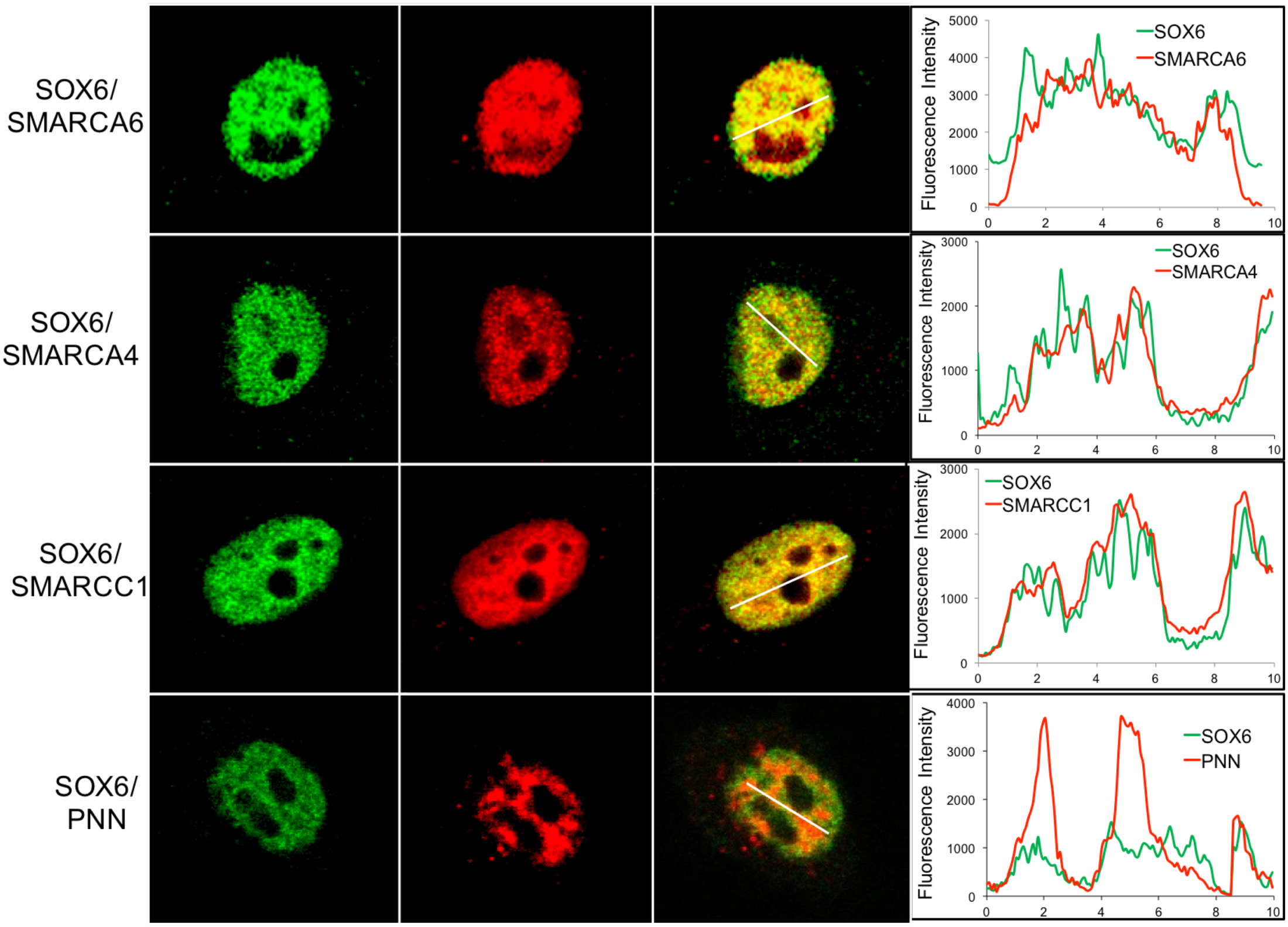

I
SOX6
IVL, SPRR2F & TGM1
SOX6
binding motif

Figure. 4

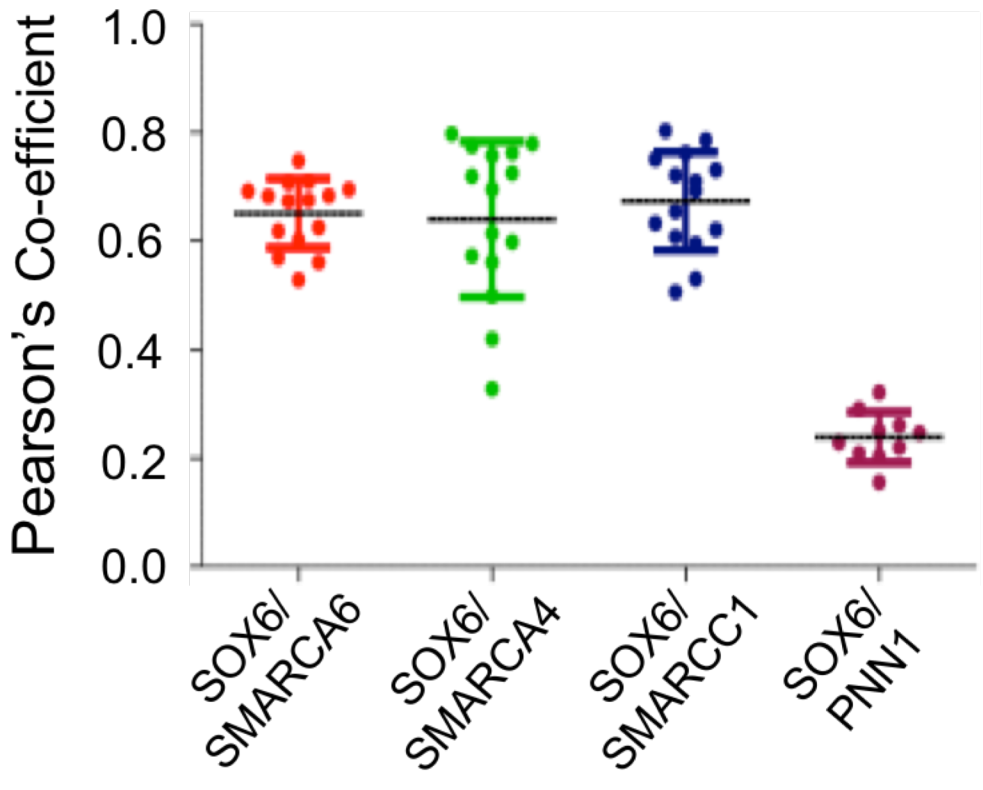
A

Protein	Other name	Full name
SMARCA4	BRG-1	SWI/SNF Related, Matrix Associated, Actin Dependent Regulator Of Chromatin Subfamily C Member 1
SMARCD2	BAF60b	SWI/SNF Related, Matrix Associated, Actin Dependent Regulator Of Chromatin, Subfamily D, Member 2
SMARCC1	BAF155	SWI/SNF Related, Matrix Associated, Actin Dependent Regulator Of Chromatin Subfamily C Member 1
SMARCA6	HELLS	SWI/SNF2-Related Matrix-Associated Actin-Dependent Regulator Of Chromatin Subfamily A Member 6
ACTL6A	BAF53	Actin Like 6A

B



C



D

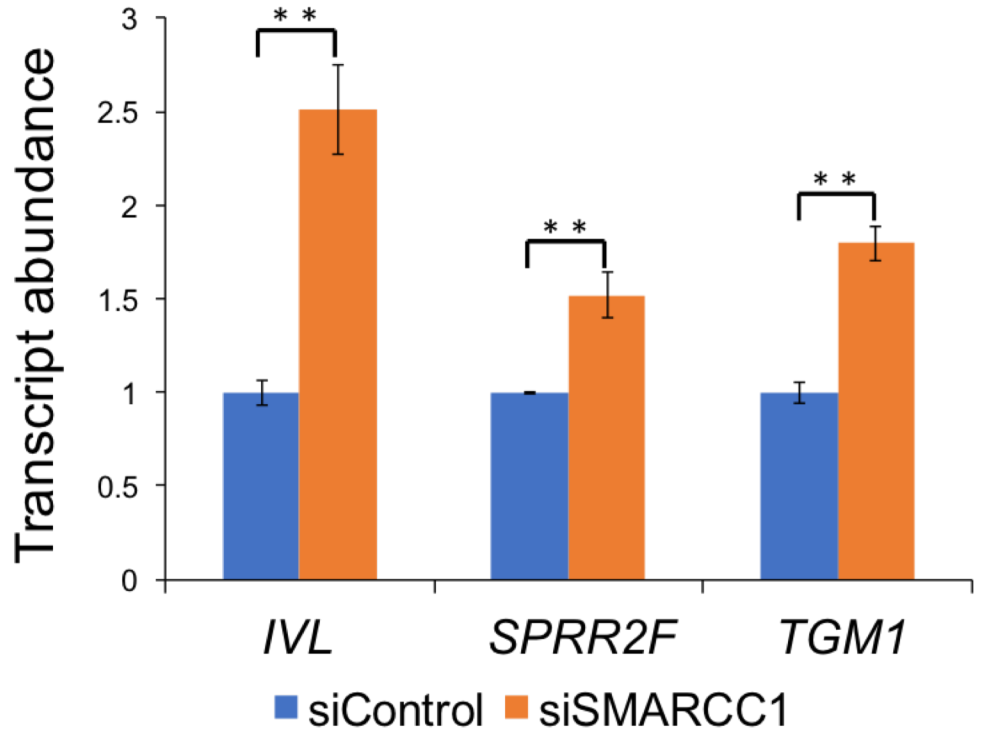
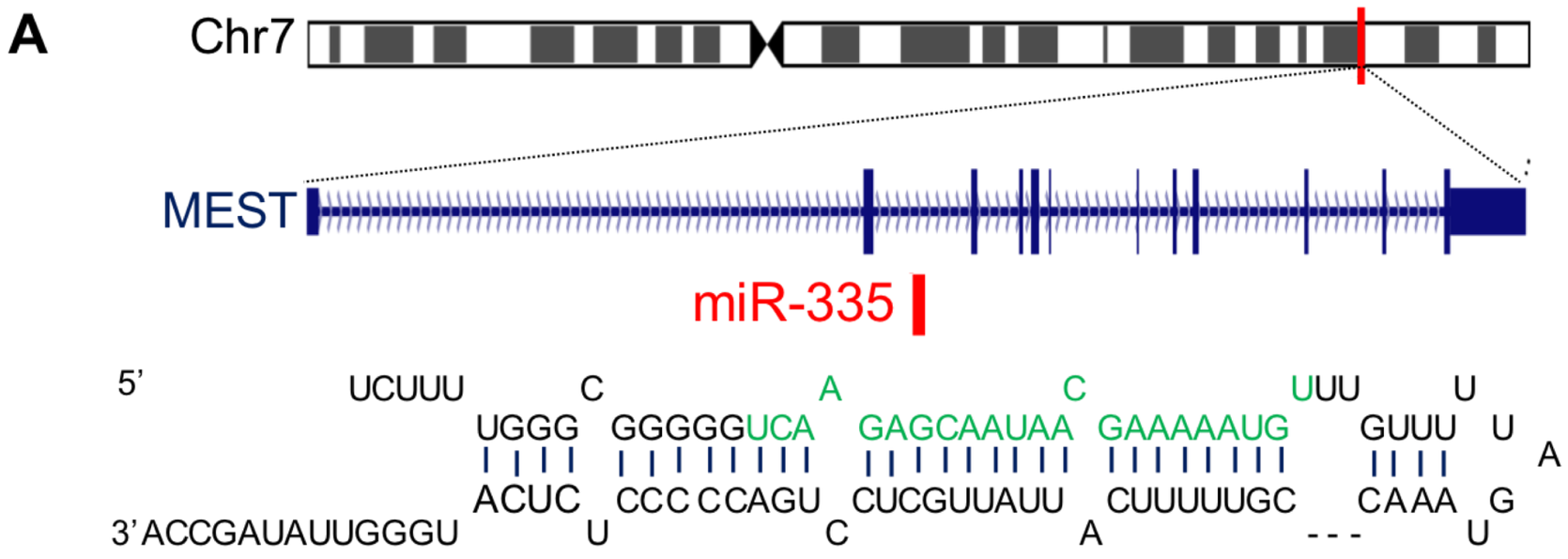
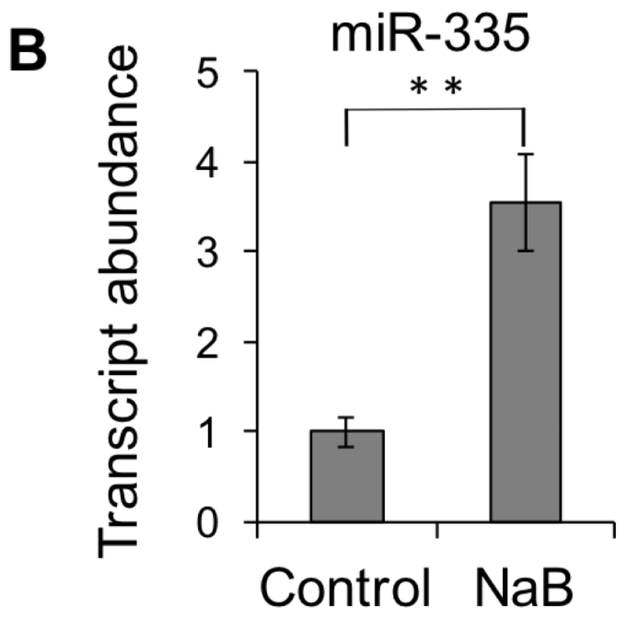
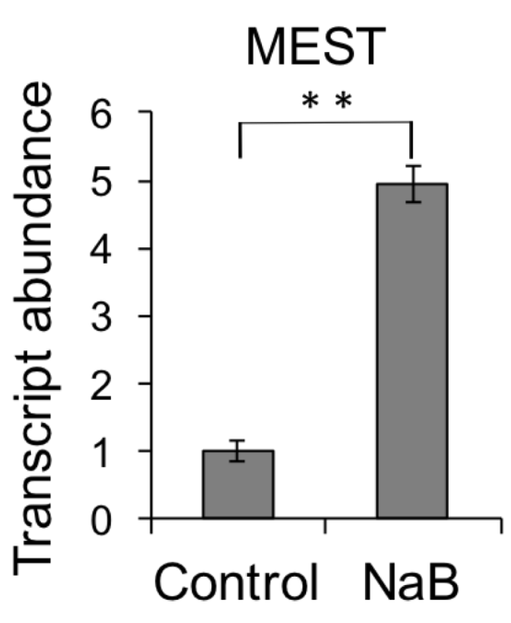
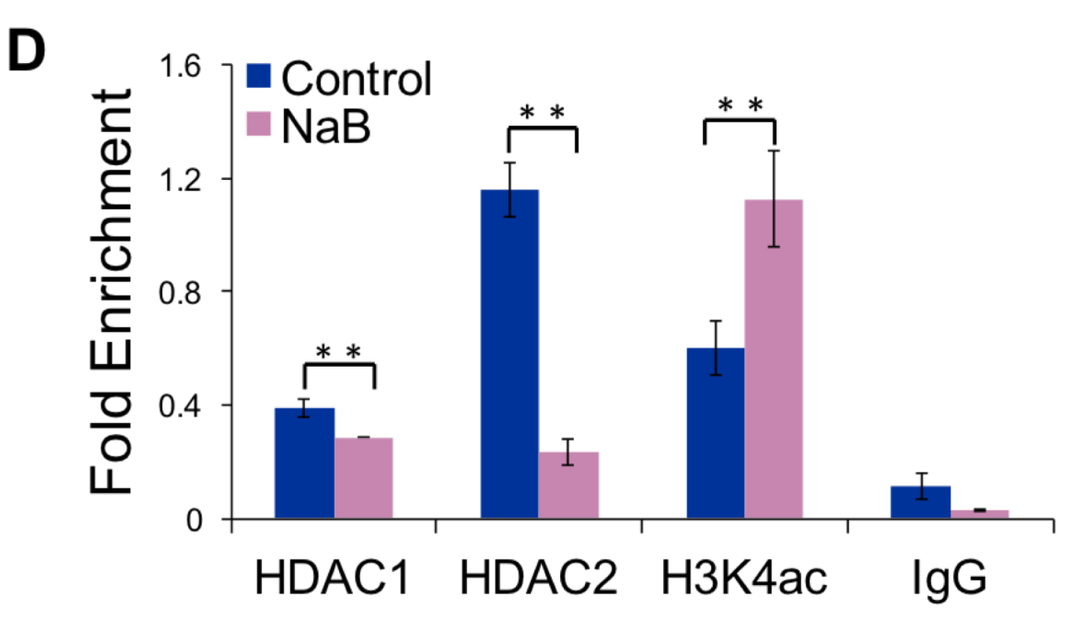


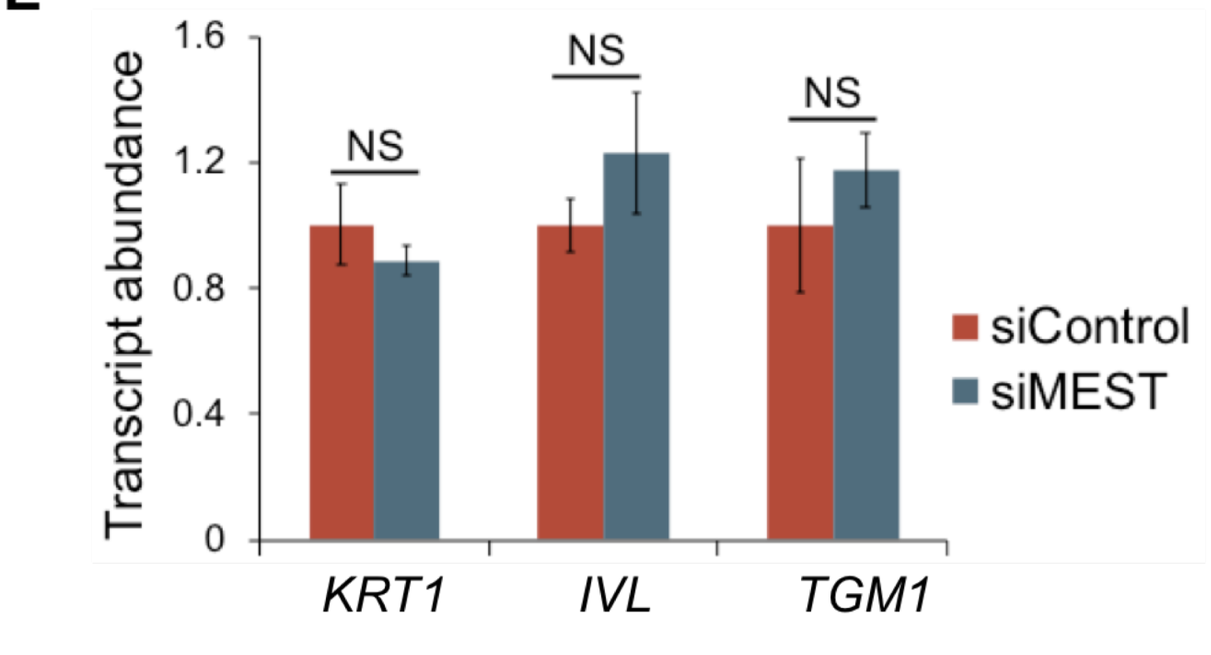
Figure. 5


A
Chr7
MEST
miR-335
5'
UCUUU C A C UUU U
UGGG GGGGGUCA GAGCAAUAA GAAAAAUG GUUU U A
ACUC CCC C CAGU CUCGUUAUU CUUUUUGC CAAA G
3' ACCGAUAUUGGGU U C A - - - U


B
miR-335
Transcript abundance
0
1
2
3
4
5
* *
Control
NaB


C
MEST
Transcript abundance
0
1
2
3
4
5
6
* *
Control
NaB


D
Fold Enrichment
0
0.4
0.8
1.2
1.6
Control
NaB
* *
* *
* *
HDAC1
HDAC2
H3K4ac
IgG


E
Transcript abundance
0
0.4
0.8
1.2
1.6
NS
NS
NS
siControl
siMEST
KRT1
IVL
TGM1

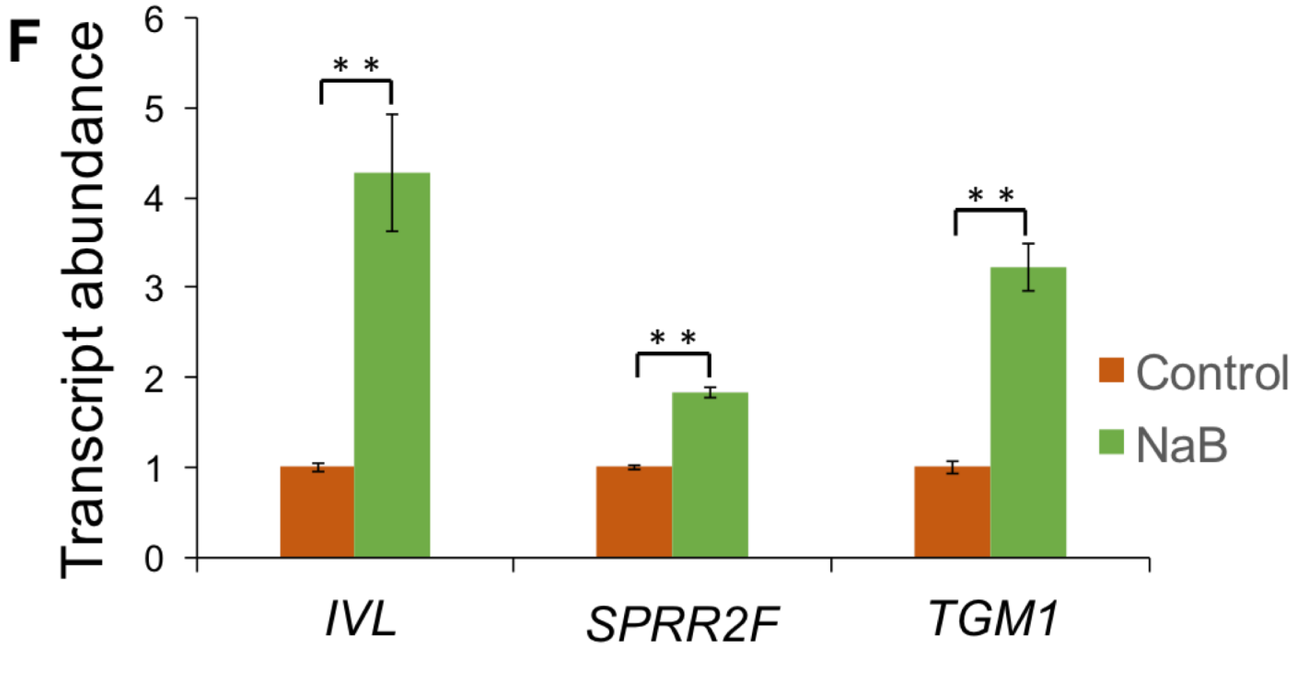
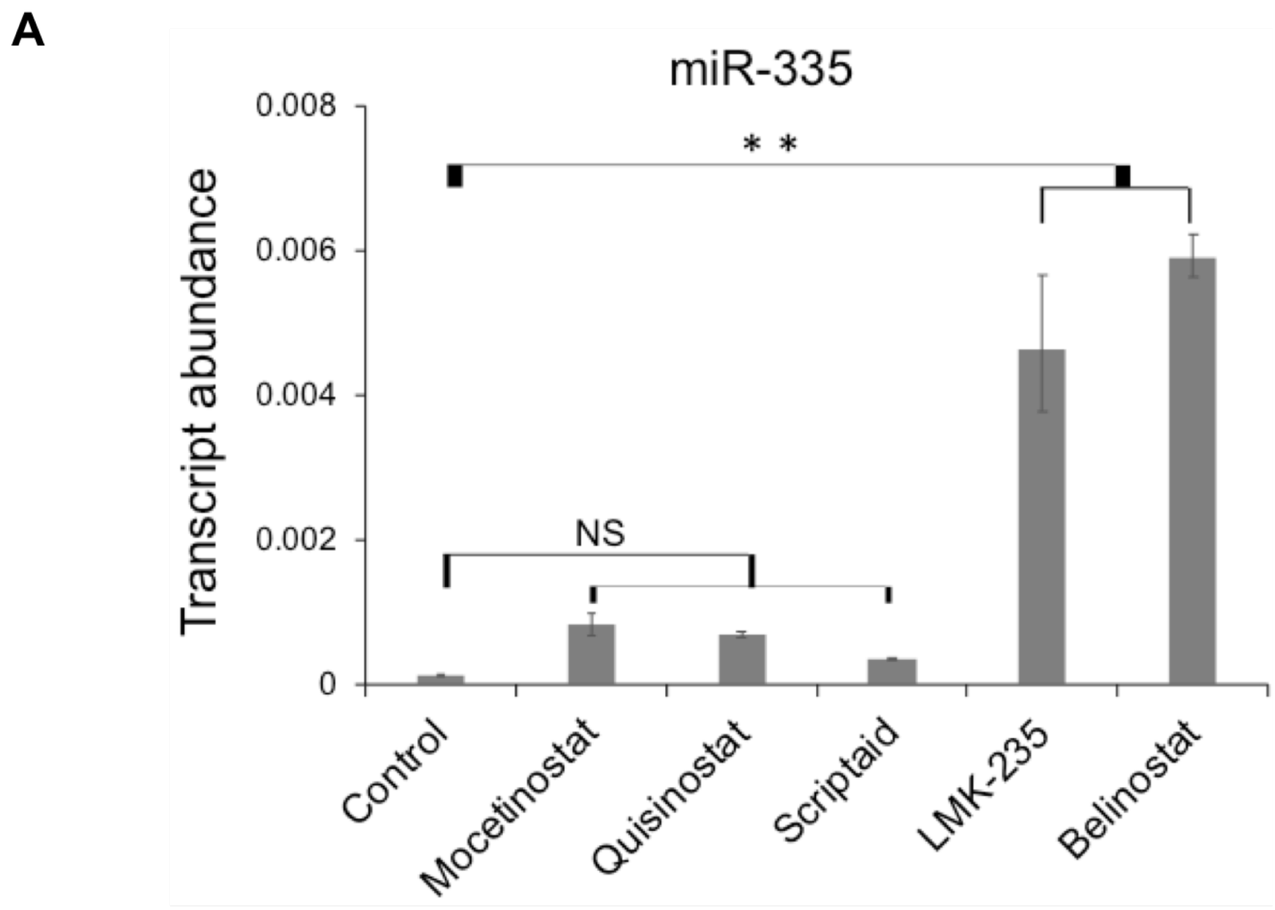
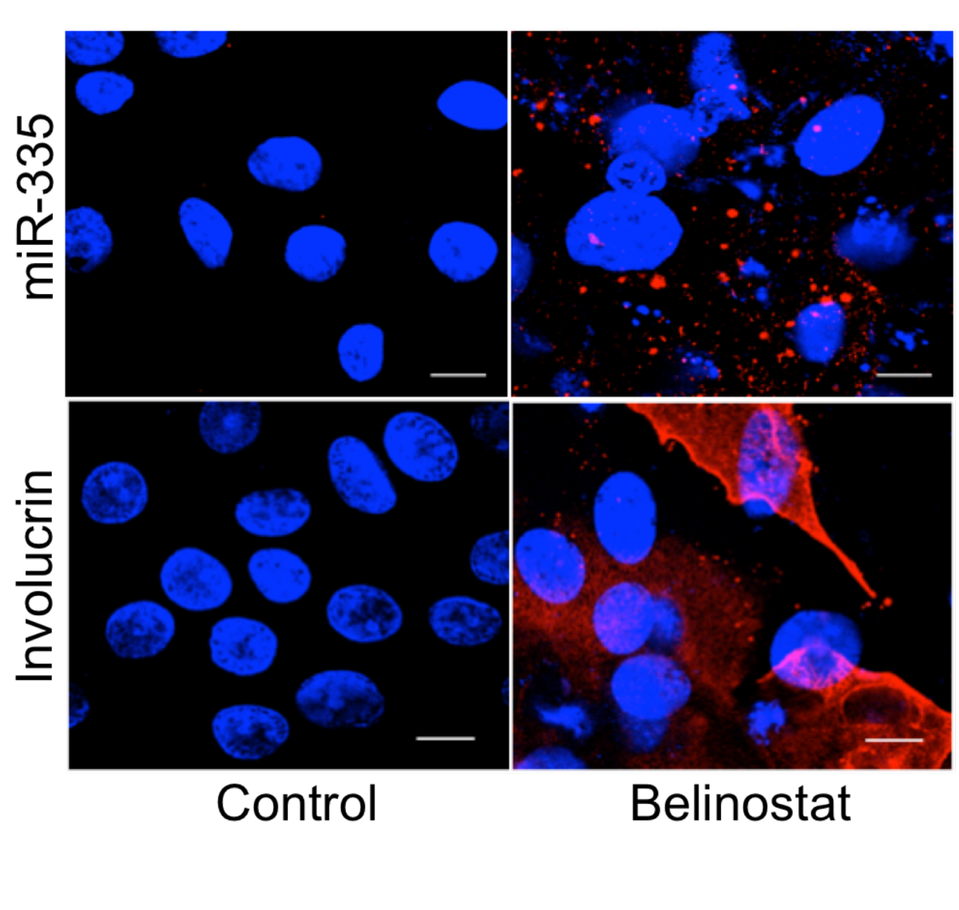
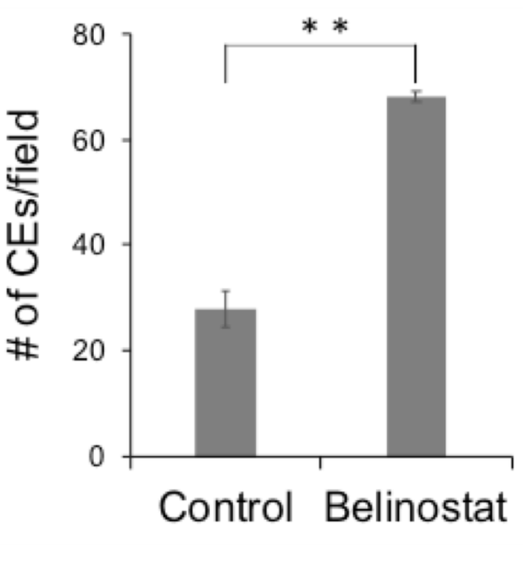
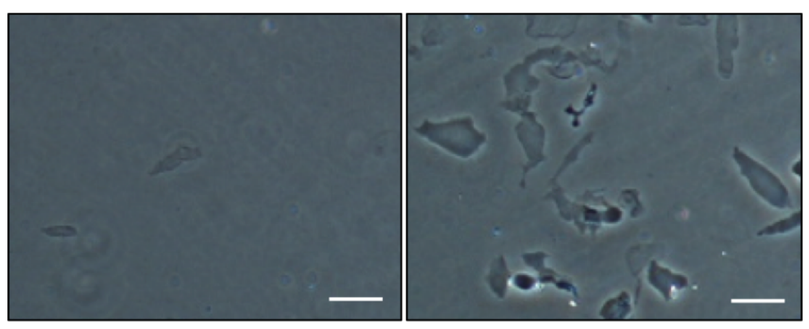

F
Transcript abundance
0
1
2
3
4
5
6
* *
* *
* *
Control
NaB
IVL
SPRR2F
TGM1

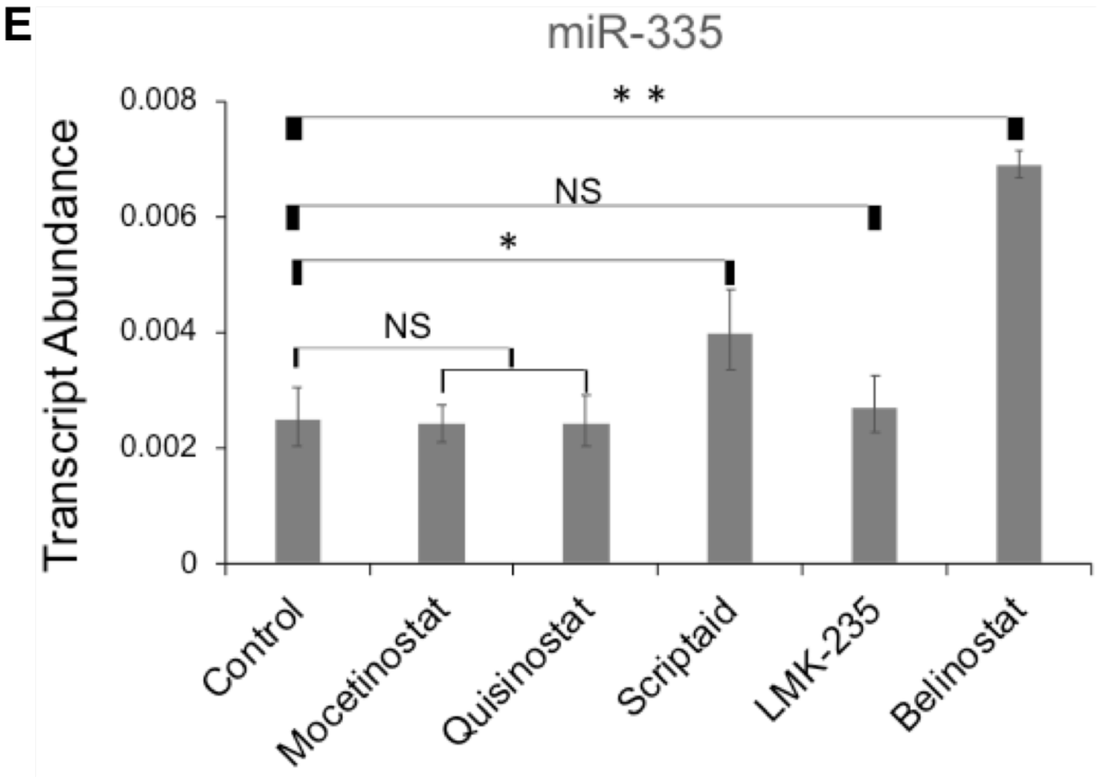
Figure. 6

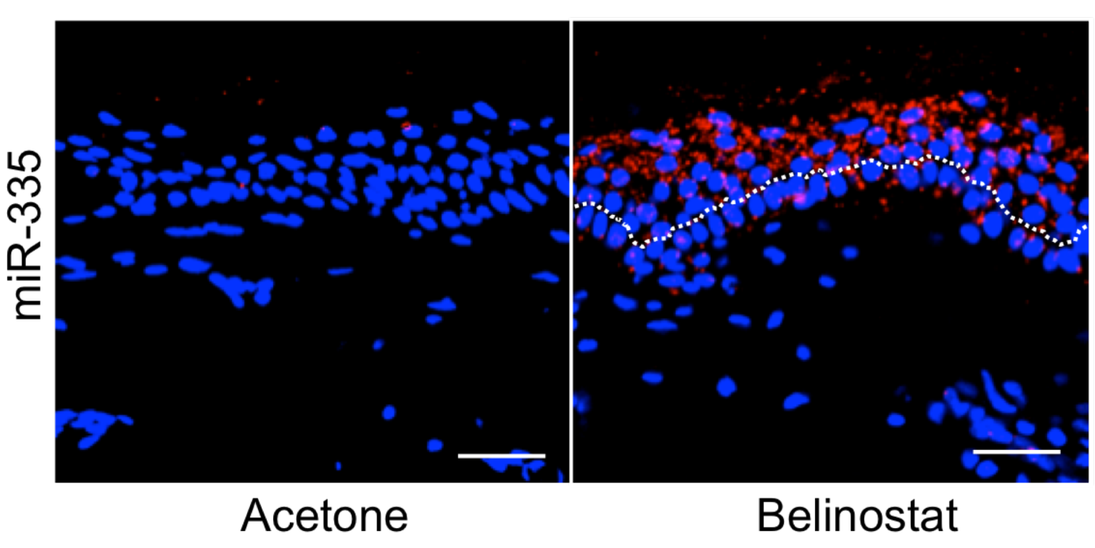

A
miR-335
Transcript abundance
0.008
0.006
0.004
0.002
0
* *
NS
Control
Mocetinostat
Quisinostat
Scriptaid
LMK-235
Belinostat

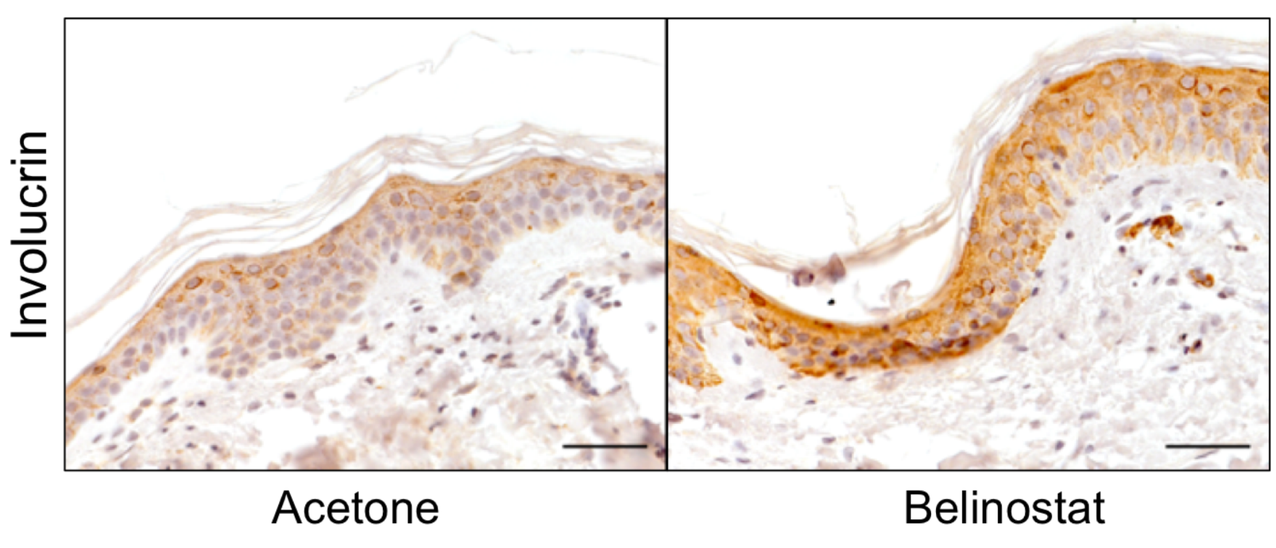

B
miR-335
Involucrin
Control
Belinostat


C
of CEs/field
80
60
40
20
0
* *
Control
Belinostat


D
Control
Belinostat


E
miR-335
Transcript Abundance
0.008
0.006
0.004
0.002
0
* *
NS
*
NS
Control
Mocetinostat
Quisinostat
Scriptaid
LMK-235
Belinostat


F
miR-335
Acetone
Belinostat


G
Involucrin
Acetone
Belinostat

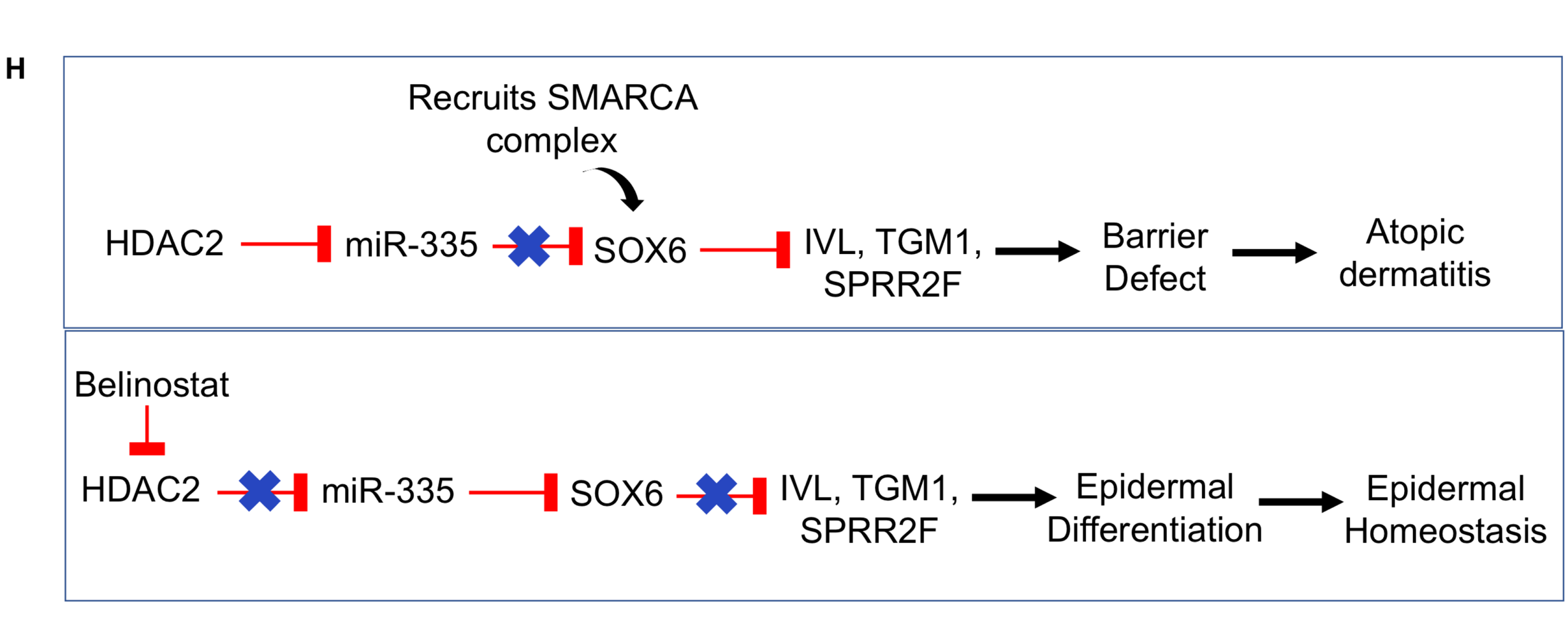

H
Recruits SMARCA complex
HDAC2
miR-335
SOX6
IVL, TGM1, SPRR2F
Barrier Defect
Atopic dermatitis
Belinostat
HDAC2
miR-335
SOX6
IVL, TGM1, SPRR2F
Epidermal Differentiation
Epidermal Homeostasis

Figure. S1

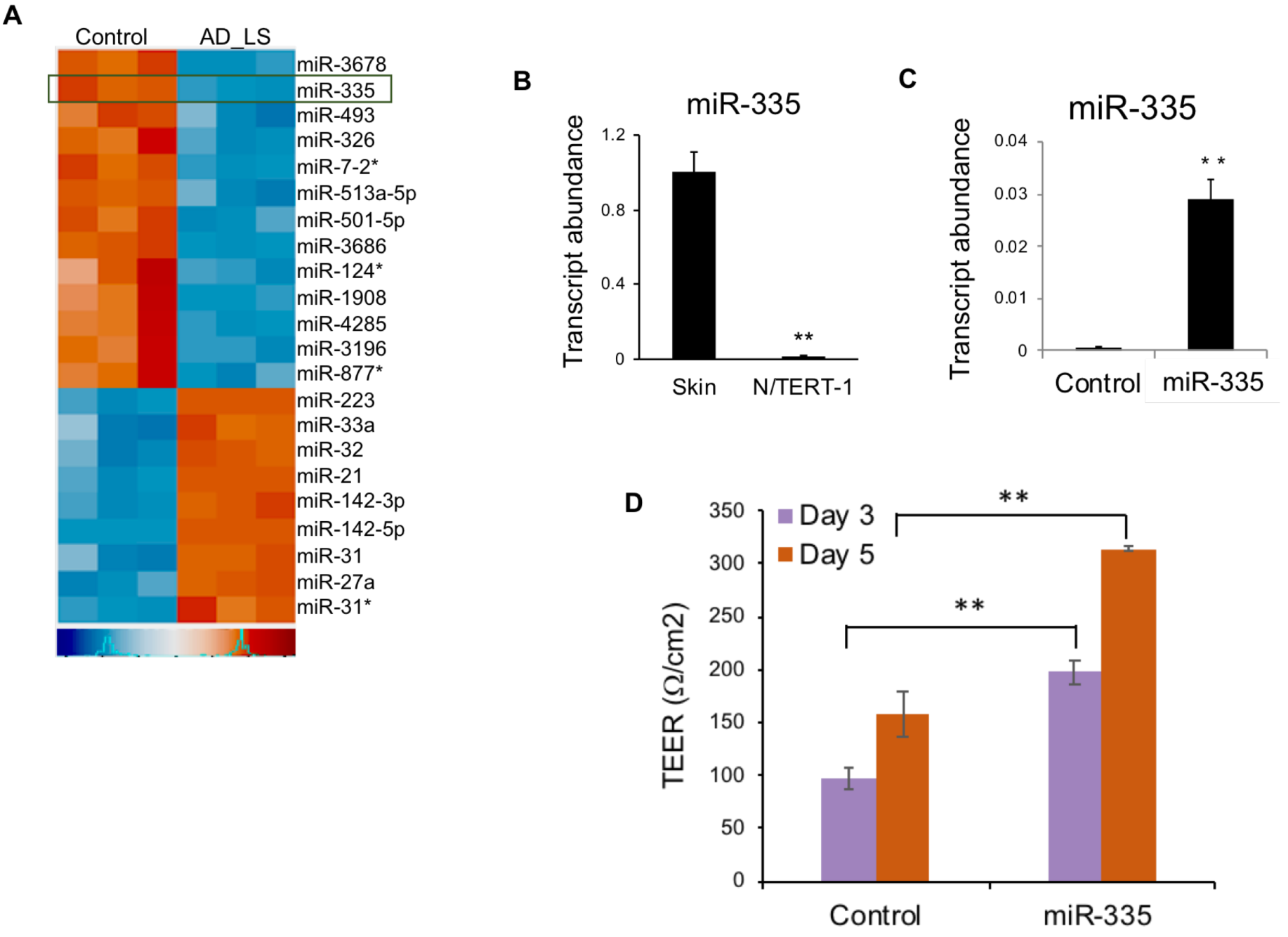

A
Control
AD_LS
miR-3678
miR-335
miR-493
miR-326
miR-7-2*
miR-513a-5p
miR-501-5p
miR-3686
miR-124*
miR-1908
miR-4285
miR-3196
miR-877*
miR-223
miR-33a
miR-32
miR-21
miR-142-3p
miR-142-5p
miR-31
miR-27a
miR-31*
B
miR-335
Transcript abundance
1.2
0.8
0.4
0
**
Skin
N/TERT-1
C
miR-335
Transcript abundance
0.04
0.03
0.02
0.01
0
* *
Control
miR-335
D
Day 3
Day 5
**
**
TEER (Ω/cm2)
350
300
250
200
150
100
50
0
Control
miR-335

Figure. S2

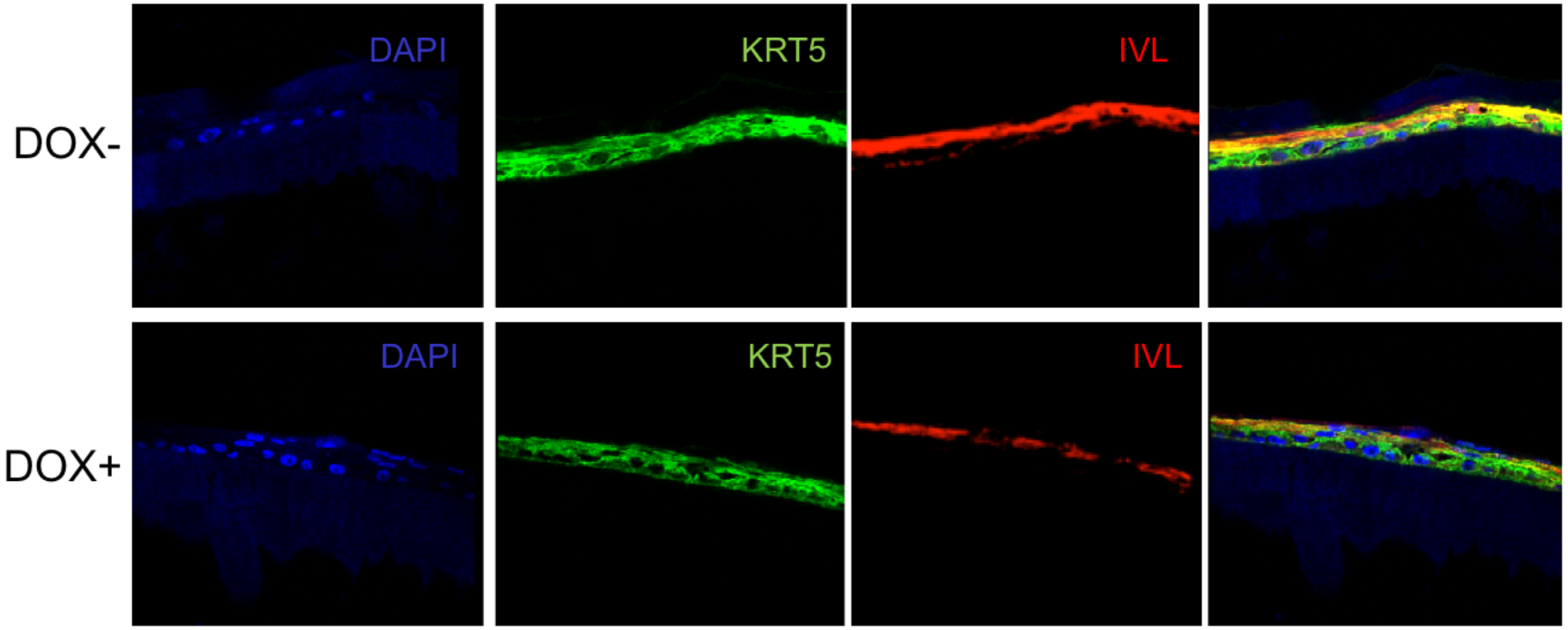
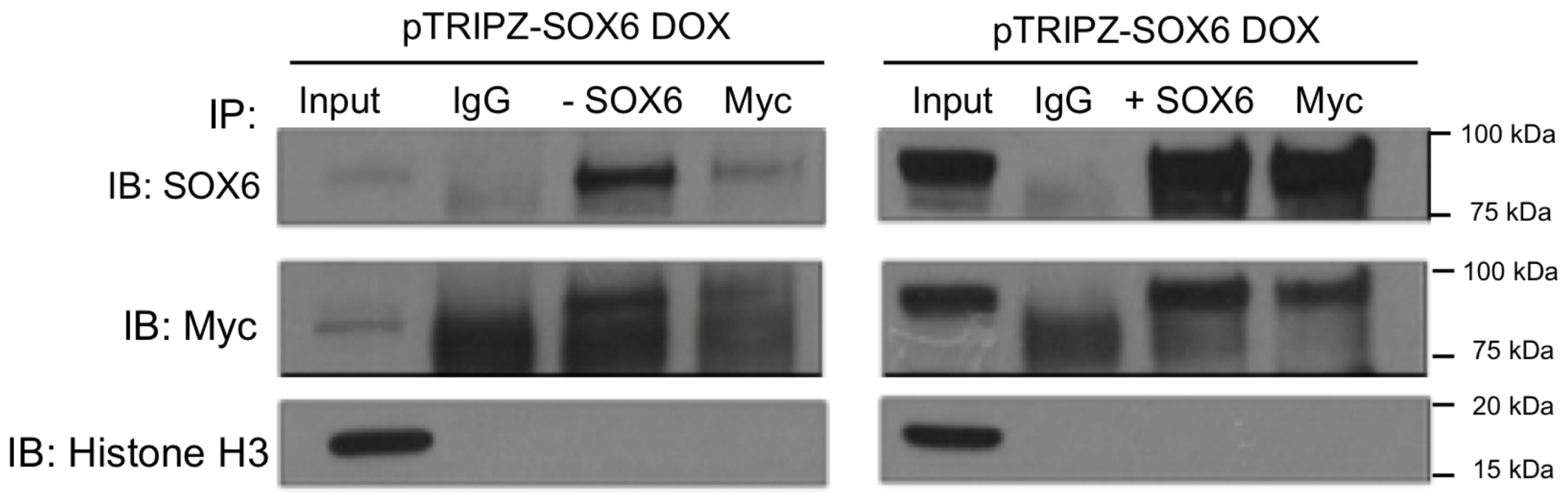


Figure. S3

A



B

	Accession	Protein name	# Unique Peptides	# Peptides	# PSMs
1	Q9NRZ9	HELLS	16	18	19
2	Q9UIG0	BAZ1B	12	22	23
3	Q03701	CEBPZ	8	11	11
4	Q9Y3T9	NOC2L	9	12	12
5	Q9BVP2	GNL3	7	11	12
6	P52948	NUP98	9	12	12
7	Q12905	ILF2	5	5	5
8	P51532	SMARCA4	7	9	9
9	O60716	CTNND1	5	10	10
10	O43159	RRP8	4	7	7
11	Q9H307	PNN	6	7	7
12	Q99459	CDC5L	3	8	8
13	Q16576	RBBP7	1	5	6
14	Q9NRL2	BAZ1A	4	8	8
15	Q92925	SMARCD2	3	6	6
16	Q9NQZ2	UTP3	3	6	6
17	O14981	BTAF1	3	7	8
18	P07199	CENPB	3	4	4
19	Q08945	SSRP1	2	4	5
20	P05412	JUN	3	4	4
21	Q9NWH9	SLTM	2	6	9
22	O94776	MTA2	2	4	4
23	P37198	NUP62	3	3	3
24	Q92922	SMARCC1	2	4	4
25	Q14527	HLTF	2	2	2
26	O96019	ACTL6A	2	3	3

C

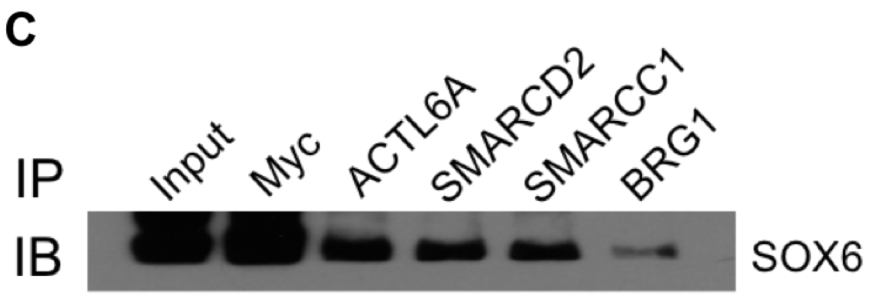


Figure. S4

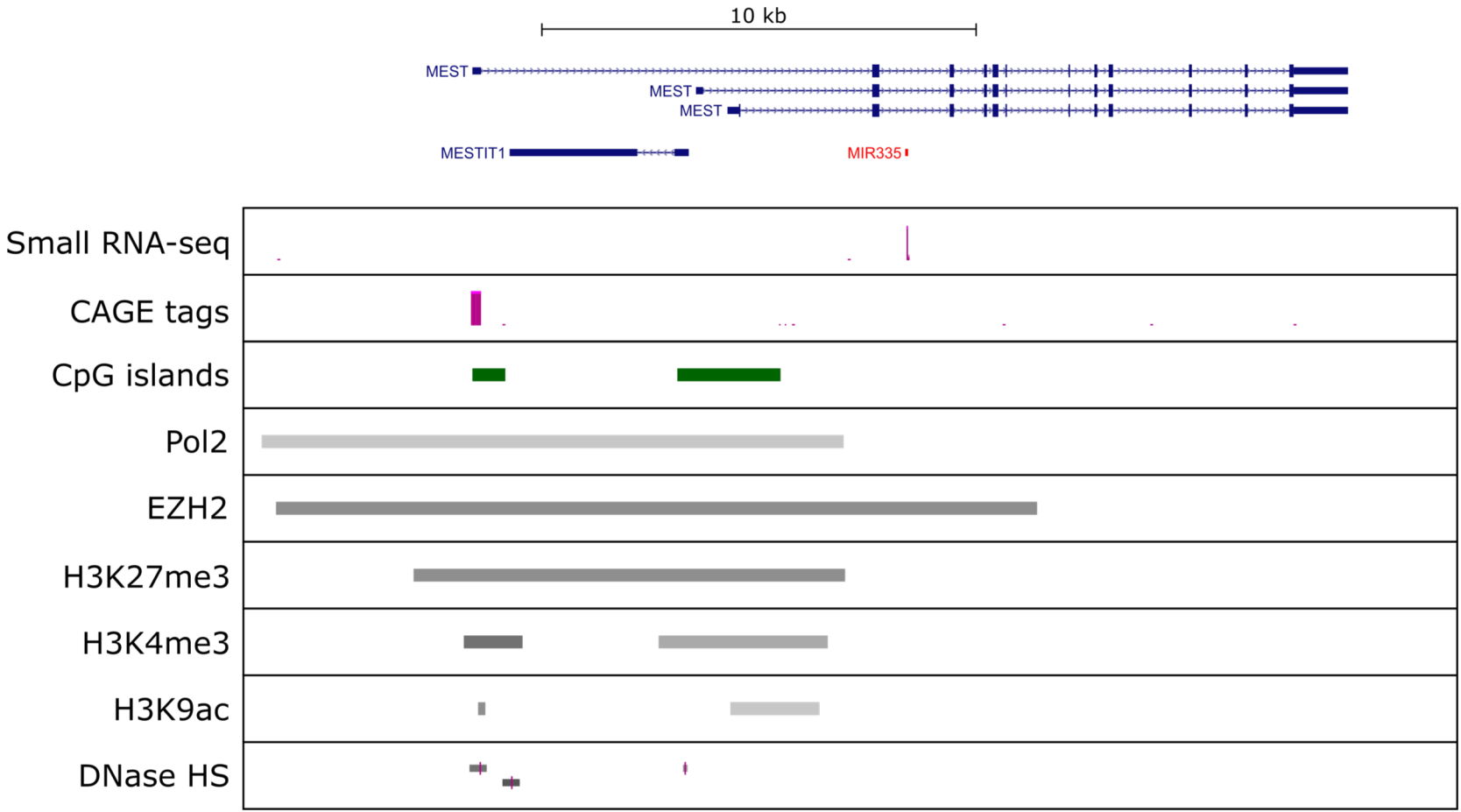
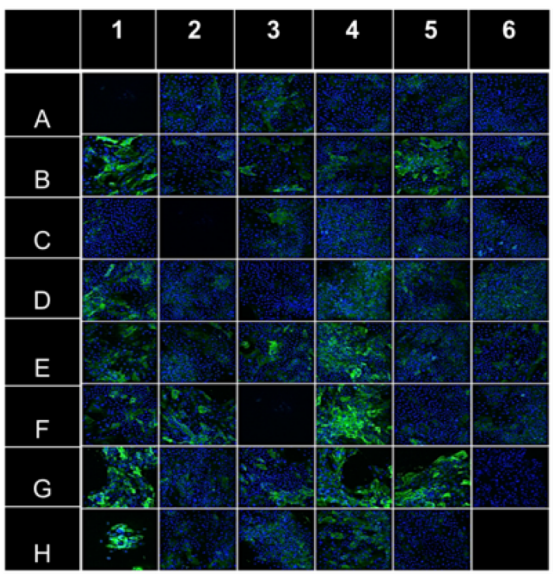

10 kb
MEST
MEST
MEST
MESTIT1
MIR335
Small RNA-seq
CAGE tags
CpG islands
Pol2
EZH2
H3K27me3
H3K4me3
H3K9ac
DNase HS

Figure. S5

A

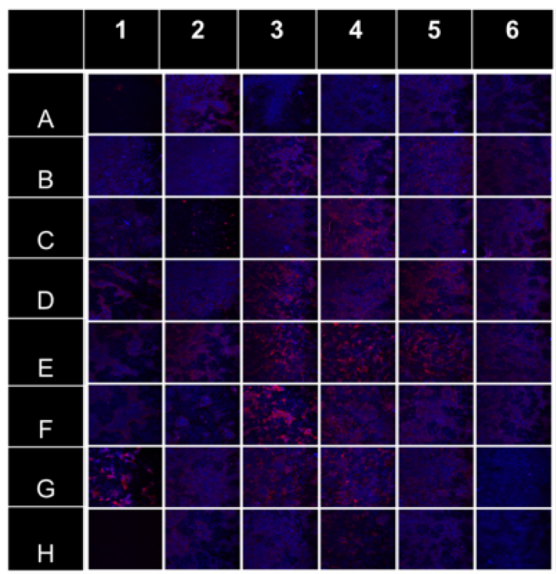
	1	2	3	4	5	6
A	Panobinostat	Mocetinostat	Givinostat	Sodium phenylbutyrate	Santacruzamate A	ITSA-1
B	Trichostatin A	Valproic acid	AR-42	RGFP966	CAY10603	Sodium butyrate
C	Vorinostat	CUDC-101	Parthenolide	HPOB	Tasquinimod	DMSO
D	Entinostat	Droxinostat	Tubastatin A HCl	RG2833	BG45	DMSO
E	**Belinostat**	MC1568	Resminostat	TMP269	BRD73954	Mock
F	Abexinostat	Pracinostat	CUDC-907	Nexturastat A	Ricolinostat	Mock
G	LAQ824	Divalproex sodium	M344	4SC-202	Scriptaid	Primary Negative
H	Quisinostat	PCI-34051	CI-994	LMK-235	Tubastatin	

B



IVL

C



SOX6

D

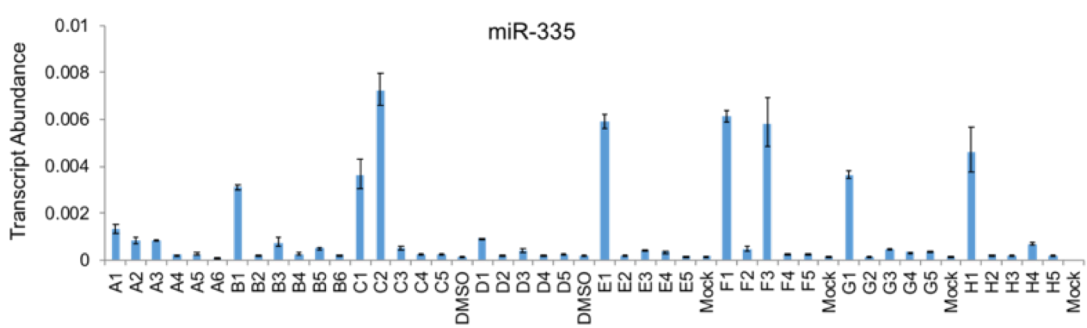


Figure. S6

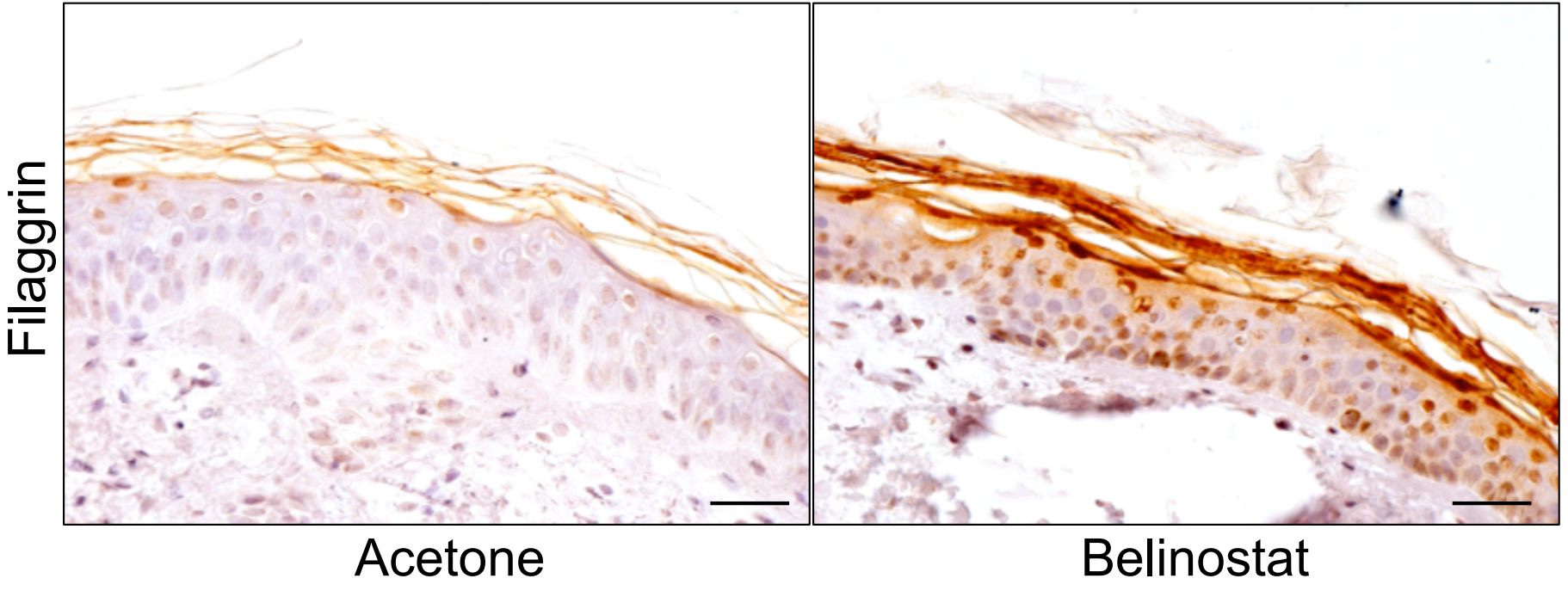


Figure. S2

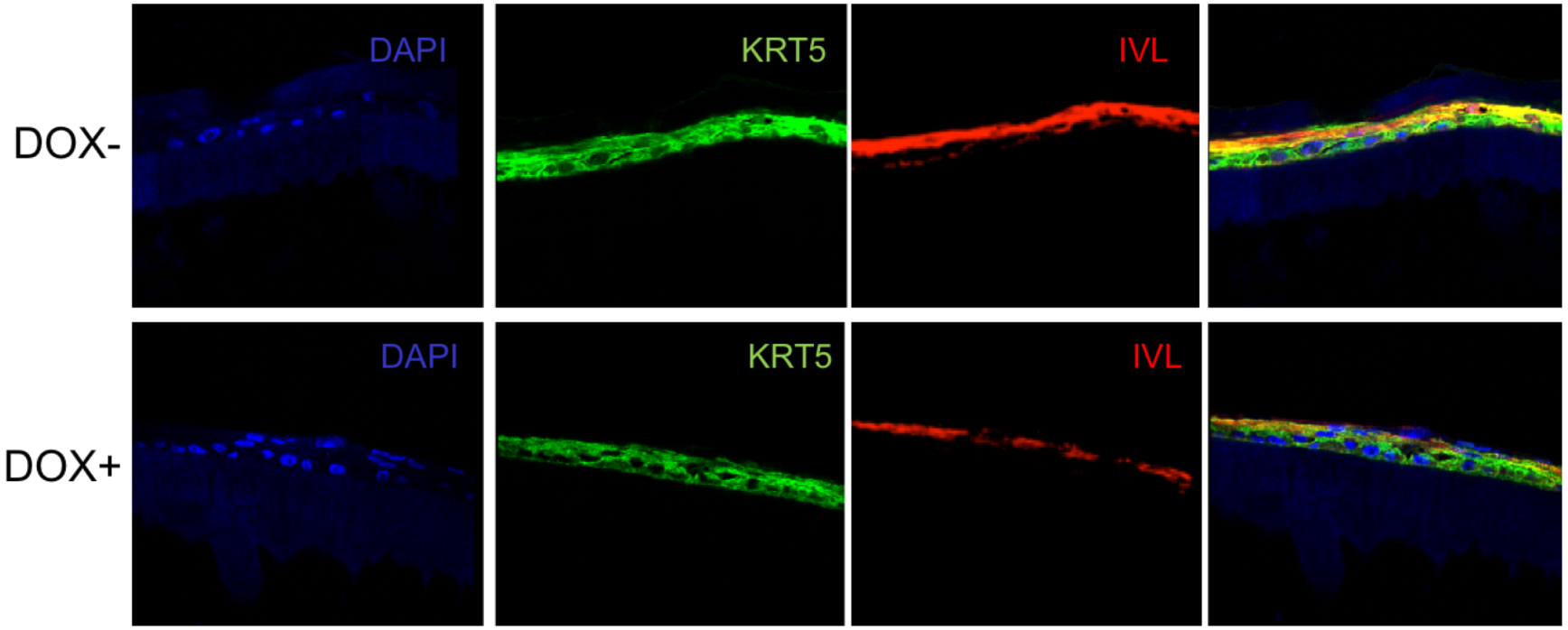
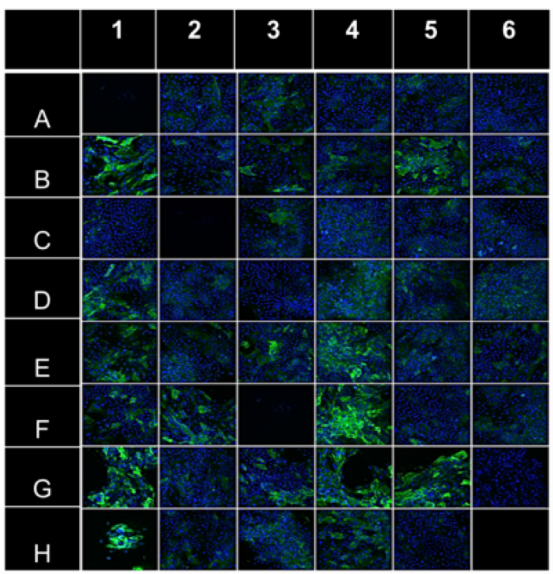


Figure. S5

A

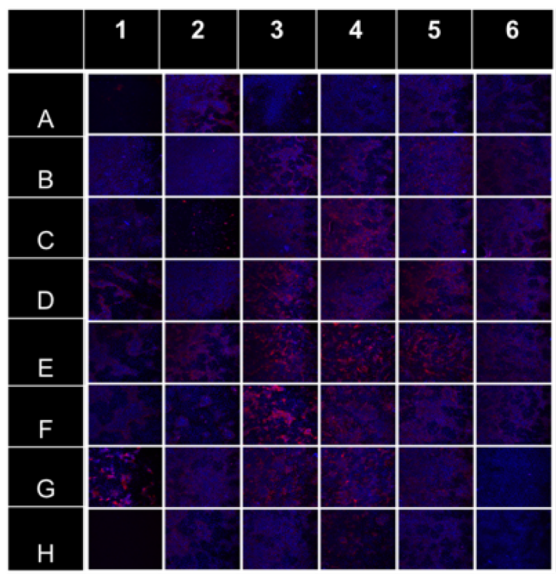
	1	2	3	4	5	6
A	Panobinostat	Mocetinostat	Givinostat	Sodium phenylbutyrate	Santacruzamate A	ITSA-1
B	Trichostatin A	Valproic acid	AR-42	RGFP966	CAY10603	Sodium butyrate
C	Vorinostat	CUDC-101	Parthenolide	HPOB	Tasquinimod	DMSO
D	Entinostat	Droxinostat	Tubastatin A HCl	RG2833	BG45	DMSO
E	**Belinostat**	MC1568	Resminostat	TMP269	BRD73954	Mock
F	Abexinostat	Pracinostat	CUDC-907	Nexturastat A	Ricolinostat	Mock
G	LAQ824	Divalproex sodium	M344	4SC-202	Scriptaid	Primary Negative
H	Quisinostat	PCI-34051	CI-994	LMK-235	Tubastatin	

B



IVL

C



SOX6

D

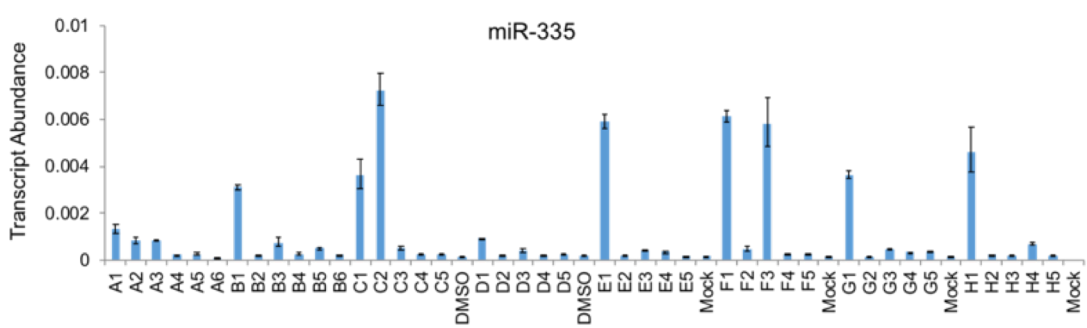


Figure. S6

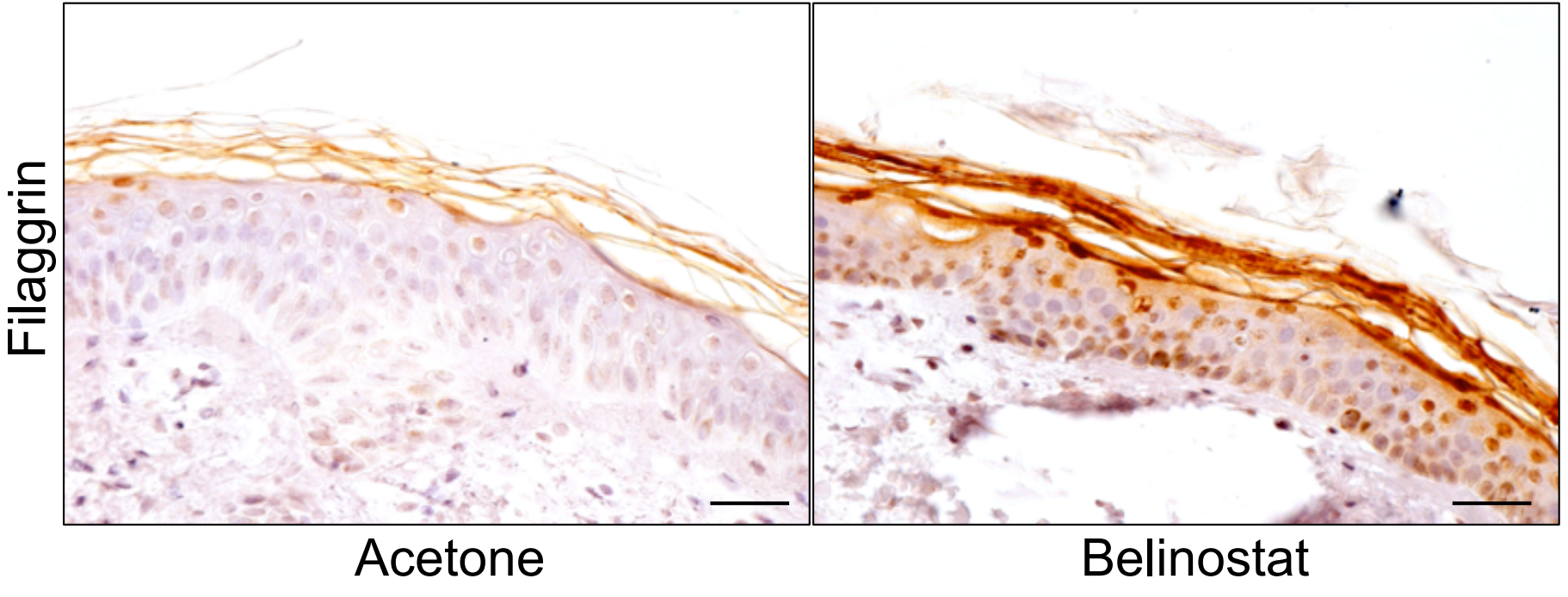
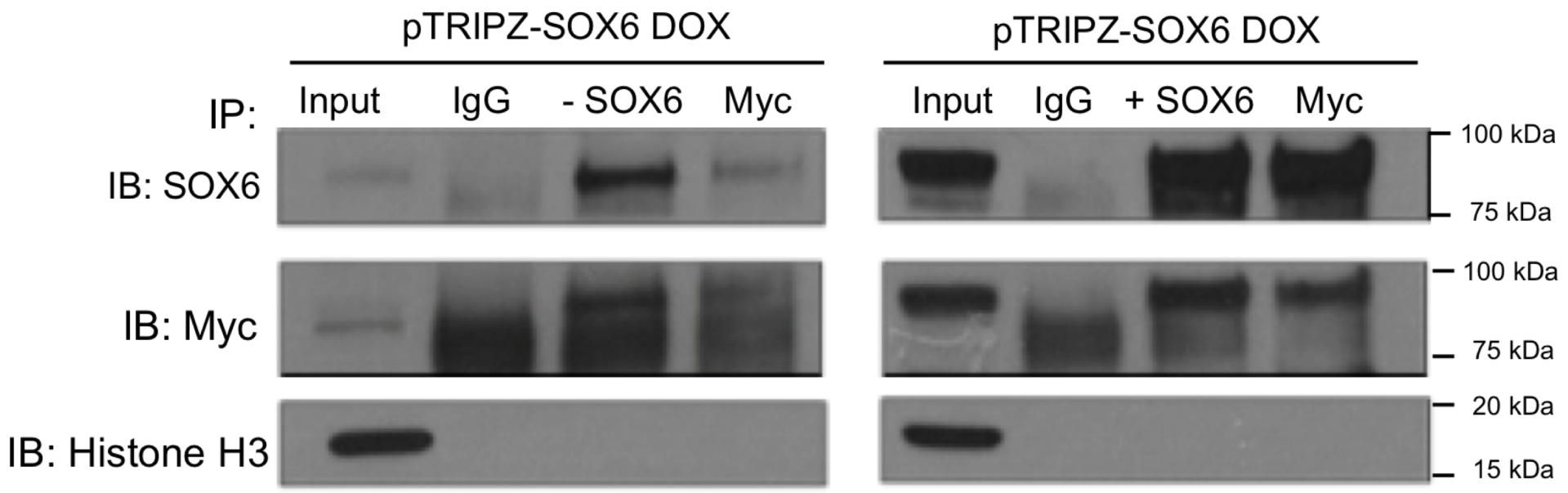


Figure. S3

A



B

	Accession	Protein name	# Unique Peptides	# Peptides	# PSMs
1	Q9NRZ9	HELLS	16	18	19
2	Q9UIG0	BAZ1B	12	22	23
3	Q03701	CEBPZ	8	11	11
4	Q9Y3T9	NOC2L	9	12	12
5	Q9BVP2	GNL3	7	11	12
6	P52948	NUP98	9	12	12
7	Q12905	ILF2	5	5	5
8	P51532	SMARCA4	7	9	9
9	O60716	CTNND1	5	10	10
10	O43159	RRP8	4	7	7
11	Q9H307	PNN	6	7	7
12	Q99459	CDC5L	3	8	8
13	Q16576	RBBP7	1	5	6
14	Q9NRL2	BAZ1A	4	8	8
15	Q92925	SMARCD2	3	6	6
16	Q9NQZ2	UTP3	3	6	6
17	O14981	BTAF1	3	7	8
18	P07199	CENPB	3	4	4
19	Q08945	SSRP1	2	4	5
20	P05412	JUN	3	4	4
21	Q9NWH9	SLTM	2	6	9
22	O94776	MTA2	2	4	4
23	P37198	NUP62	3	3	3
24	Q92922	SMARCC1	2	4	4
25	Q14527	HLTF	2	2	2
26	O96019	ACTL6A	2	3	3

C

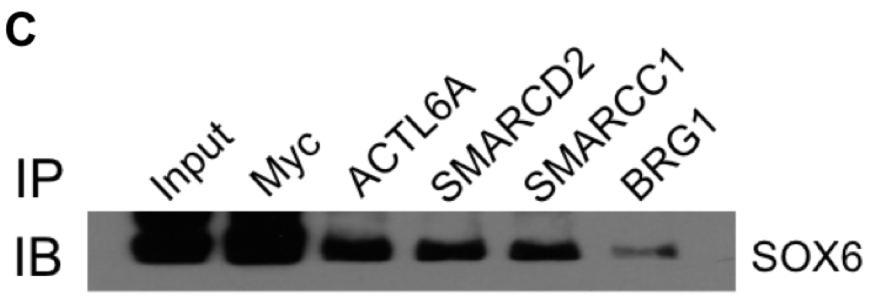
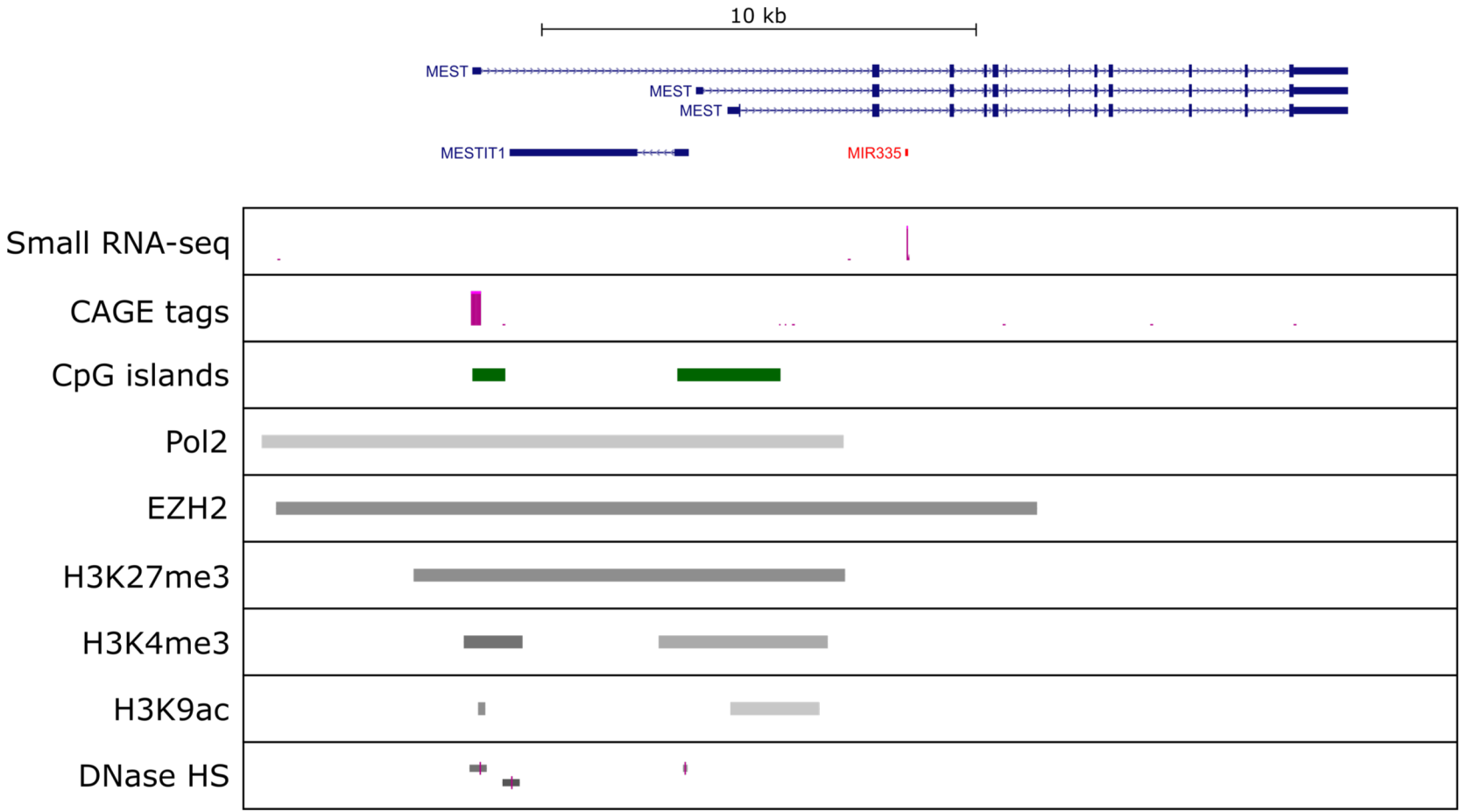


Figure. S4


10 kb
MEST
MEST
MEST
MESTIT1
MIR335
Small RNA-seq
CAGE tags
CpG islands
Pol2
EZH2
H3K27me3
H3K4me3
H3K9ac
DNase HS

Journal Pre-proof

Supplementary Information

For

Belinostat resolves skin barrier defects in atopic dermatitis by targeting the dysregulated miR-335:SOX6 axis

Wen Chiy Liew, PhD[1,2,5], Gopinath M. Sundaram, PhD[1,2], Shan Quah, PhD[1], Lum Guo Guang, B.Sc.[1], Jonathan S.L. Tan, B.Sc.[1], Rajkumar Ramalingam, PhD[2], John E. A. Common, PhD[1], Mark B. Y. Tang, MD[3], E. Birgitte Lane, PhD[1], Steven Thng, MBBS[1,4], Prabha Sampath, PhD[1,5,6,*]

Table. S1: List of antibodies used

Antibody	Company	Catalog number	Species	Dilution	Application
SOX6	R&D Systems	MAB7759	Mouse	1:300	IHC & ICC
				2 µg	IP
	Bethyl	A303-553A	Rabbit	2 µg	ChIP
				2 µg	IP
	Millipore	AB5805	Rabbit	1:800	Western blot
				1:200	IHC & ICC
c-Myc	Sigma-Aldrich	C3956	Rabbit	1:800	Western blot
				2 µg	IP
Involucrin	Novacastra	NCL-IVL	Mouse	1:200	IHC & ICC
				1:800	Western blot
Beta-actin	Millipore	12-370	Rabbit	2 µg	IP
Histone H3	Cell signalling technology	4499	Rabbit	2 µg	ChIP
Rabbit IgG	Millipore	12-371B	Mouse	2 µg	IP
				2 µg	ChIP
Mouse IgG	Abcam	ab7028	Rabbit	2 µg	ChIP
	Abcam	ab7029	Rabbit	2 µg	IP
HDAC1	Invitrogen	PA5-64099	Rabbit	1:100	ICC

HDAC2	Abcam	ab7029	Rabbit	1:100	ICC
HELLS	Abcam	ab51256	Rabbit	1 µg	IP
BAZ1B	Cell signalling	49360	Rabbit	1:100	ICC
				1:100	ICC
SMARCA4	Sigma-Aldrich	HPA001378	Rabbit	1:100	ICC
			Rabbit	1 µg	IP
PNN	Abcam	ab8106	Rabbit	1 µg	IP
			Rabbit	1:100	ICC
SMARCC1	Bethyl	A301-319A	Rabbit	1 µg	IP
			Rabbit	1: 100	ICC

Table. S2: shRNA Oligo Sequences

shRNA	Sequence
SOX6_sh4_O1F	GATCCGACAGGAGATGAGGCAGTTCT
SOX6_sh4_O1R	ACTCGAGTAGAACTGCCTCATCTCCTGTCG
SOX6_sh4_O2 F	ACTCGAGTAGAACTGCCTCATCTCCTGTCTTTTTTCCAAG
SOX6_sh4_O2R	AATTCTTGGAAAAAAGACAGGAGATGAGGCAGTTCT

Table. S3: Primer Sequences for Cloning

Clone	Forward primer	Reverse primer
pTRIPZ_SOX6	GACACCGGTCGCCACC*ATGCAG AAACTCATCTCAGAAGAGGATCT* GATGTCTTCCAAGCAAGCCACC	GTCACGCGTTTAGTTGG CACTGACAGCCTC
pCDH_miR335	TCGATCTAGAACCACCATTGGTT CTCTCTCC	TCGAGAATTCCTGGAAG TAACCCAAGCCAAC

Table. S4: Primer sequences for ChIP-qPCR

Primer Name	Forward primer sequence	Reverse primer sequence
IVL	GCTTAAGATGCCTGTGGTGAG	CAGGAGTCAGGGCACTCTTTA
TGM1	CAGCTTCTTCATCCGGGAGAA	AATGGGGAGAAGATGCTAGGG
SPRR2F	CCCTTGACCACCAGTTAGAGA	CTGGGTTAAGTGCTCCTGACT
RPLP0	CTCAGAGCAAGCTCCTCCAAC	AACGAATACAGGCAACCATTG
KRT14	AGCCCAAAACACTCCAAACAA	AATTGGAAAGGGATGCGAGTG
MEST	TAAGGAAAGAGTTGGGGCACT	CCCTCTAACAGTGGCTCCTTT
miR-335	TCTCTCTCCTTACCATCCCTGA	GCCTGGCATATGGTAATTACTG

Table. S5: Primers used for real time PCR

Primer Name	Forward primer sequence	Reverse primer sequence
CNFN	CTCACCTTTTGTCTGCCCTG	TTGTGGGTGTATTTCTGGCAG
IVL	TGGCCACCCAAACATAAATAA	ACCCTCACCCCATTAAAGAGA
TGM1	GGAGCACCTGAACCATGATTC	ACTTCATGTAGACCAGGCCAT
SPRR1A	ACACCCTACTCCATTCTGCTT	CCAGAATGAGGGTAAGGGACA
SPRR1B	TCAATAGTCACTCCAGCACCA	TGGGATAGGGGATTCAGCATC
SPRR2A	CCACCGAAGAGCAAGTAACAG	TGGCAGCCTCAGAAAAGAAAC
SPRR2E	CAGCTTCACCTGCATCTTCTC	CACCTGGACAGTGGCAATATG
SPRR2F	CTGGTACCTAAGCACCGATCT	GGACTGTGGACACTTTGATGG
SPRR3G	CATGTCCTTCAACGGTCACTC	CTATGGCTTGGGGTGACAATG
KRT1	AACTTGCAGCAGTCCATCAGT	GGTGTTCATCAGCTCCTGGTA
SOX6	AAAGCTTCGGATTGGGGAGTA	CACCTGTTCCTGTGGTGATTG
MEST	ATGGGCCATTGGATCCTGTAA	AGAAGGAGTTGATGAAGCCCA
RPLP0	CAGATTGGCTACCCAACTGTT	GGGAAGGTGTAATCCGTCTCC
SMARCC1	CCAATGCCAGGAAACATCTTA	ATCTTCCAGGCTAAGGAGCAG

Journal Pre-proof

Journal Pre-proof

Table. S6: Differentially expressed miRNAs in normal vs AD LS

miRNA	Log_2 FC	Adjusted p-value
hsa-miR-335	-2.05071	7.55E-10
hsa-miR-451	-2.02619	3.58E-09
hsa-miR-4290	-1.70415	9.71E-09
hsa-miR-4285	-1.60556	3.38E-07
hsa-miR-4268	-1.5807	1.57E-08
hsa-miR-3687	-1.53107	1.44E-09
hsa-miR-483-3p	-1.48269	6.85E-08
hsa-miR-4279	-1.46726	3.88E-08
hsa-miR-326	-1.40212	3.88E-08
hsa-miR-7-2*	-1.36727	1.24E-08
hsa-miR-3196	-1.3481	6.92E-07
hsa-miR-513a-5p	-1.33315	1.90E-07
hsa-miR-501-5p	-1.17405	2.11E-07
hsa-miR-493	-1.15678	2.48E-06
hsa-miR-99a	-1.09175	9.85E-08
hsa-miR-1908	-1.07471	2.25E-06
hsa-miR-124*	-1.03648	3.96E-06
hsa-miR-3686	-1.01967	4.79E-08
hsa-miR-877*	-1.01245	1.83E-06
hsa-miR-3175	0.997334	1.47E-06
hsa-miR-32	0.997533	3.05E-07
hsa-miR-21*	1.010585	0.007811
hsa-miR-3621	1.037089	3.14E-07
hsa-miR-223	1.053103	5.17E-08
hsa-miR-31*	1.064144	1.11E-05
hsa-miR-33a	1.232449	1.83E-06
hsa-miRPlus-C1110	1.278948	0.000107
hsa-miR-27a	1.345597	2.78E-08

Journal Pre-proof

hsa-miR-31	1.631136	3.31E-07
hsa-miR-142-5p	1.867304	7.55E-10
hsa-miR-142-3p	2.05951	3.58E-09
hsa-miR-21	2.758994	7.55E-10

Table. S6: Differentially expressed miRNAs were identified based on $\log_2$ FC ≥ 1 or ≤ -1 and adjusted p-value < 0.05 from microarray analysis

Supplementary Figure Legends:

Figure. S1: Differential expression of miR-335 in AD lesional skin: A) Heat-map of selected genes generated from microRNA microarray using total RNA from AD lesional skin samples in comparison with RNA from normal human skin samples. Expression values displayed in shades of red (high) or blue (low) relative to the individual mean value of the gene in linear scale. **B)** Relative transcript abundance of miR-335 in normal human skin versus N/TERT-1 keratinocyte cells, represented as a bar graph (n=3). **C)** Relative transcript abundance of miR-335 in N/TERT-1 cells transfected with miR-335 mimics versus control cells, represented as a bar graph (n=4). **D)** Bar graphs represent transepithelial electrical resistance (TEER) measured on day-3 and day-5 in N/TERT-1 cells transfected with control RNA or miR-335 mimics (n=3) ***P*<0.001 versus control.

Figure. S2: SOX6 targets IVL: Inducible expression of SOX6 leads to significant downregulation of IVL which is essential for keratinocyte differentiation and cornification as depicted in an organotypic assay.

Figure. S3: SOX6 interacts with the SMARCA complex: A) Immunoprecipitation of SOX6 protein from nuclear extracts of HEK293T cells transfected with pTRIPZ-SOX6 in the presence of doxycycline, followed by western blot analysis with indicated antibodies. Extracts were immunoprecipitated with rabbit IgG antibodies, antibodies to SOX6 or Myc. **B)** List of potential SOX6 interacting partners. **C)** Immunoprecipitation with specific antibodies of SWI/SNF complex followed by western blot analysis for SOX6. Myc serves as a positive control.

Figure. S4: Promoter analysis of MEST/miR-335 locus: CAGE tags are only present in the upstream region of MEST, but not miR-335, suggesting that miR-335 does not have an independent promoter.

Figure S5: Belinostat induces expression of miR-335: A) Table shows the list of HDAC inhibitors library (Selleckchem) and their treatment regimen in 96 well plate. **B)** Cells treated with HDAC inhibitors were fixed and subjected to immunocytochemistry with antibodies

specific to IVL. **C)** Cells treated with HDAC inhibitors were fixed and subjected to immunocytochemistry with antibodies specific to SOX6. Images were acquired from each well using a fluorescent microscope at identical acquisition settings. **D)** Relative transcript abundance of miR-335 in N/TERT-1 cells either mock treated or treated with HDAC inhibitors.

Figure. S6: Belinostat restores barrier function and FLG expression: Immunohistochemical analysis of FLG, on sections from human skin biopsies that were topically treated with acetone alone or belinostat dissolved in acetone. Scale bars, 50 µm.

Journal Pre-proof